GEOLOGY OF THE INTERMOUNTAIN WEST
an open-access journal of the Utah Geological Association
ISSN 2380-7601
Volume 7 *2020*

RHYOLITE IGNIMBRITE BOULDERS AND COBBLES IN THE MIDDLE JURASSIC CARMEL FORMATION OF UTAH AND ARIZONA—AGE, COMPOSITION, TRANSPORT, AND STRATIGRAPHIC SETTING

Bart J. Kowallis, Douglas A. Sprinkel, Eric H Christiansen, Skylor Steed, and David F. Wheatley

GEOLOGY OF THE INTERMOUNTAIN WEST

an open-access journal of the Utah Geological Association

ISSN 2380-7601

Volume 7 ***2020***

Editors

Douglas A. Sprinkel
Azteca Geosolutions
801.391.1977
GIW@utahgeology.org
dsprinkel@gmail.com

Bart J. Kowallis
Brigham Young University
801.422.2467
bkowallis@gmail.com

Steven Schamel
GeoX Consulting, Inc.
801.583-1146
geox-slc@comcast.net

Thomas C. Chidsey, Jr.
Utah Geological Survey
801.537.3364
tomchidsey@utah.gov

John R. Foster
Utah Field House of
Natural History State Park
Museum
435.789.3799
eutretauranosuchus@
gmail.com

Production

Cover Design and Desktop Publishing
Douglas A. Sprinkel

Cover

Large, rounded igneous, boulder-sized clast from near where sample WH-1 was collected in the White House area, Kane County, Utah. The boulder has broken into several large pieces having maximum diameters of 1.3, 1.0, and 0.8 m with several other 0.5 m blocks and is compositionally similar to other igneous clasts in the area. These igneous clasts are weathered out from debris-flow beds within the Paria River Member of the Carmel Formation. David Wheatley for scale. Photograph by Mark Hansford.

UGA Board

2020 President	Leslie Heppler	lheppler@utah.gov	801.538.5257
2020 President-Elect	Riley Brinkerhoff	riley.brinkerhoff@gmail.com	406.839.1375
2020 Program Chair	Paul Inkenbrandt	paulinkenbrandt@utah.gov	801.537.3361
2020 Treasurer	Greg Gavin	greg@loughlinwater.com	801.538.4779
2020 Secretary	Elliot Jagniecki	ejagniecki@utah.gov	801.537.3370
2020 Past President	Peter Nielsen	peternielsen@utah.gov	801.537.3359

UGA Committees

Environmental Affairs	Craig Eaton	eaton@ihi-env.com	801.633.9396
Geologic Road Sign	Greg Gavin	greg@loughlinwater.com	801.541.6258
Historian	Paul Anderson	paul@pbageo.com	801.364.6613
Membership	Rick Ford	rford@weber.edu	801.626.6942
Outreach	Greg Nielsen	gnielsen@weber.edu	801.626.6394
Public Education	Zach Anderson	zanderson@utah.gov	801.537.3300
	Matt Affolter	gfl247@yahoo.com	
Publications	Paul Inkenbrandt	paulinkenbrandt@utah.gov	801.537.3361
Publicity	Paul Inkenbrandt	paulinkenbrandt@utah.gov	801.537.3361
Social/Recreation	Roger Bon	rogerbon@xmission.com	801.942.0533

AAPG House of Delegates

2017–2020 Term	Tom Chidsey	tomchidsey@utah.gov	801.537.3364

State Mapping Advisory Committee

UGA Representative	Bill Loughlin	bill@loughlinwater.com	435.649.4005

Earthquake Safety Committee

Chair	Grant Willis	gwillis@utah.gov	801.537.3355

UGA Website — www.utahgeology.org

Webmaster	Paul Inkenbrandt	paulinkenbrandt@utah.gov	801.537.3361

UGA Newsletter

Newsletter Editor	Bill Lund	uga.newsletter@gmail.com	435.590.1338

Become a member of the UGA to help support the work of the Association and receive notices for monthly meetings, annual field conferences, and new publications. Annual membership is $20 and annual student membership is only $5. Visit the UGA website at www.utahgeology.org for information and membership application.

The UGA board is elected annually by a voting process through UGA members. However, the UGA is a volunteer-driven organization, and we welcome your voluntary service. If you would like to participate please contact the current president or committee member corresponding with the area in which you would like to volunteer.

Utah Geological Association formed in 1970 from a merger of the Utah Geological Society, founded in 1946, and the Intermountain Association of Geologists, founded in 1949. Affiliated with the American Association of Petroleum Geologists.

GEOLOGY OF THE INTERMOUNTAIN WEST
an open-access journal of the Utah Geological Association
Volume 7 ***2020***

Rhyolite Ignimbrite Boulders and Cobbles in the Middle Jurassic Carmel Formation of Utah and Arizona—Age, Composition, Transport, and Stratigraphic Setting

Bart J. Kowallis[1], Douglas A. Sprinkel[2], Eric H Christiansen[1], Skylor Steed[1], and David F. Wheatley[3]
[1]*Department of Geological Sciences, Brigham Young University, Provo, UT 84604 (bkowallis@byu.edu)*
[2]*Azteca Geosolutions, Pleasant View, UT 84414 and Utah Geological Survey, Salt Lake City, UT 84114; dsprinkel@gmail.com*
[3]*Department of Geology and Geophysics, University of Utah, Salt Lake City, UT 84112; davidfwheatley@gmail.com*

ABSTRACT

A stratigraphic layer containing rhyolite cobbles and boulders in the Middle Jurassic Carmel Formation of southern Utah represents a singular, unusual event in the otherwise low-energy sedimentation of this formation. A laser-fusion, single-crystal $^{40}Ar/^{39}Ar$ age of 171.73 ± 0.19 Ma obtained from sanidine in one of the clasts is about 8 m.y. older than a zircon U-Pb age obtained on a fallout tuff from the sediments surrounding the clasts (163.9 ± ~3.3 Ma). The volcanic clasts are poorly-welded rhyolite ignimbrites that may have been deposited as much as 200 km from the eruptive center, perhaps along pre-existing valleys. The tuff deposits then remained in place for several million years during which time they were subjected to weathering, alteration, and perhaps topographic inversion, creating mesas capped with tuff underlain by soft Middle Jurassic silt and mud. Triggered by unusual rainfall or earthquakes, debris flows carried the clasts a few 10s of kilometers from their outcrops to the depositional site. Earlier work proposed that the Middle Jurassic arc was a low-standing, arc-graben. If this was the case, then the tectonic setting was likely similar to the modern Central American arc in the vicinity of Nicaragua where tuffs erupted from a low-standing arc deposited onto an adjacent highland and were then eroded by streams flowing to the east onto a fluvial plain that is near the sea.

INTRODUCTION

The Middle Jurassic (163–174 Ma) of the Western Cordillera was a time of active arc magmatism, leaving behind volcanic and plutonic rocks within the arc that have been widely studied (Dunne, 1986; Karish and others, 1987; Busby-Spera, 1988; Busby-Spera and others, 1990; Dunne and Walker, 1993; Riggs and others, 1993; Schermer and Busby, 1994; Fackler-Adams and others, 1997; Sorensen and others, 1998; Fohey-Breting and others, 2010; Tosdal and Wooden, 2015; Barth and others, 2017). In addition, ash beds preserved in more distal sedimentary environments have provided further insights into the character and frequency of eruptions along the Jurassic arc (Wright and Dickey, 1963; Marvin and others, 1965; Nielson, 1988; Everett and others, 1989; Christiansen and others, 1994, 2015; Blakey and Parnell, 1995; Zhang, 1996; Kowallis and others, 2001; Dickinson and others, 2010; Sprinkel and others, 2011; Doelling and others, 2013.

Chapman (1987, 1989, 1993), Marzolf (1990), and

Citation for this article.
Kowallis, B.J., Sprinkel, D.A., Christiansen, E.H, Steed, S., and Wheatley D.F., 2020, Rhyolite ignimbrite boulders and cobbles in the Middle Jurassic Carmel Formation of Utah and Arizona—age, composition, transport, and stratigraphic setting: Geology of the Intermountain West, v. 7, p. 69–96, appendix, https://doi.org/10.31711/giw.v7.pp69-96.

Blakey and Parnell (1995) reported on volcanic pebbles, cobbles, and boulders ranging in size from 2.5 cm to 2.6 m in the upper member of the Carmel Formation (equivalent to the Thousand Pockets and Paria River Members; see Doelling and others, 2013) in southern Utah and northern Arizona (figure 1). Chapman (1987, 1989) described the clasts as rhyolitic, welded tuffs (ignimbrites) with quartz, sanidine, biotite, plagioclase, hornblende, and magnetite, but having almost all the plagioclase replaced by calcite and the hornblende replaced by iron oxides. Based upon directional transport indicators in the enclosing sedimentary rocks, the clasts were transported north and northeast into the Carmel Formation depositional basin (Chapman, 1989; Blakey and Parnell, 1995).

But how did cobble- and boulder-sized clasts travel from somewhere near the western continental margin Jurassic volcanic arc to their current depositional location? Chapman (1993) proposed that debris flows generated by huge floods carried the cobbles and boulders as much as 250 to 300 km from their source in the arc to their present depositional site (palinspastically corrected for later extension), but acknowledged the unresolved problem of how large boulders could move over such large distances. Blakey and Parnell (1995) suggested that now-eroded outcrops of these volcanic rocks may have only been several kilometers from the sites of boulder and cobble deposition. But Blakey and Parnell (1995) did not explain why outcrops of ignimbrite might have been so close to the depositional sites when eruptive centers must have been 250 to 300 km away as Chapman (1993; Luscombe, 2018) recognized. A similar problem of source for coarse volcanic detritus (up to 25 cm+ diameter) occurs in the Triassic Chinle Formation (Stewart and others, 1972; Dodge, 1973). Stewart and others (1986) suggested that one possible solution to the problem was tectonic removal of the source by strike-slip offset along a major shear system cutting between the source area and the deposits. However, this does not seem to be a reasonable solution for the Middle Jurassic deposits. Chapman (1987) examined several possibilities including: (1) the magmatic source was closer to the Colorado Plateau at the time of clast deposition than the palinspastic reconstruction estimate of 250 to 300 km; (2) a broad, now eroded, volcanic apron existed around the arc region bringing source material closer to the depositional sites of the clasts; (3) transport might have been enhanced by paleovalleys that helped to extend ash-flow and debris-flow runout distances; and (4) an undiscovered Jurassic volcanic complex existed much closer to the Colorado Plateau with deposits that lapped up onto the plateau (similar to the proposal of Blakey and Parnell, 1995).

In this paper we review the stratigraphic setting of the volcanic clasts, re-examine their composition, texture, and age, then, using these data, re-examine possible solutions to the problem of transport distance between the volcanic arc and depositional basin.

MIDDLE JURASSIC STRATIGRAPHY OF THE SOUTHERN KAIPAROWITS BASIN

The Kaiparowits Basin of south-central Utah is one of several Laramide basins on the Colorado Plateau (figure 1). Middle Jurassic formations exposed in the basin and surrounding region include (in ascending stratigraphic order) the Temple Cap Formation, Carmel Formation, and Entrada Sandstone (figure 2). The Temple Cap Formation unconformably overlies the Lower Jurassic Navajo Sandstone. It was deposited on the eroded Navajo in what was identified as the J-2 unconformity by Pipiringos and O'Sullivan (1978) but is now considered to be the J-1 unconformity because of regional stratigraphic work of Sprinkel and others (2011) and Doelling and others (2013). The Temple Cap Formation is well exposed in southwestern and south-central Utah. The formation irregularly thins eastward from about 120 m in the St. George area (about 150 km west of the study area) to about 8 m in the Lake Powell area (about 50 km east of the study area), but is locally missing across the paleotopographic high of the Kaibab uplift (Peterson and Pipiringos, 1979; Wright and others, 1979; Doelling and others, 2013). The Temple Cap Formation is seemingly missing within the study area but is present about 7 km to the southeast at Judd Hollow (Sprinkel and others, 2011; Doelling and others, 2013), suggesting the easternmost flank of the Kaibab uplift extends into this area. Thin fallout tuffs in the Temple Cap Formation in the region provided $^{40}Ar/^{39}Ar$ (sanidine and biotite) and U-Pb (zircon) ages that range from 172.93 ± 0.56 to

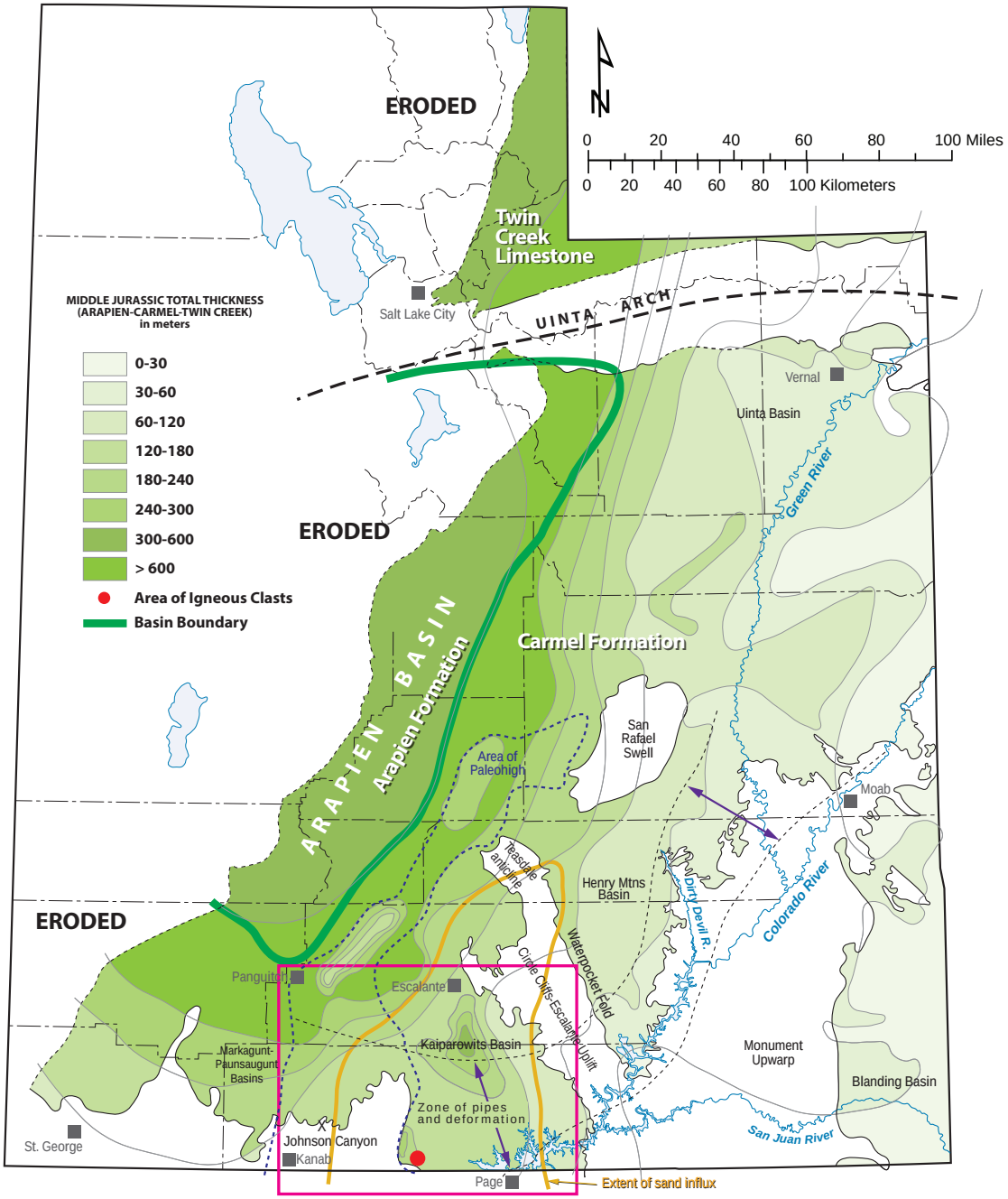

Figure 1. Paleogeologic map of Utah showing relationships for the Middle Jurassic along with the location of the igneous clasts in the Paria River Member of the Carmel Formation, southwestern part of the Kaiparowits Basin (modified from Doelling and others, 2013). The map also depicts the area of sand influx that formed the Thousand Pockets Member and is responsible for the sandy nature of the other Carmel members. The Middle Jurassic Carmel Formation (and equivalent strata) generally thins from west to east; however, note that the Carmel thins across a paleohigh that stretches from the western margin of the Kaiparowits Basin northeastward to the western flank of the San Rafael Swell. The paleotopography developed on the Lower Jurassic Navajo Sandstone on which the Middle Jurassic Temple Cap Formation was irregularly deposited; in some areas along the paleohigh, the Temple Cap is missing. The red box shows the area enlarged in figure 3. Also shown is a zone of pipes and deformed beds in Permian to Cretaceous strata (between dashed lines), the width approximately shown by the purple arrows (Wheatley and Chan, 2013, 2018; Wheatley and others, 2016; Wheatley, 2018.

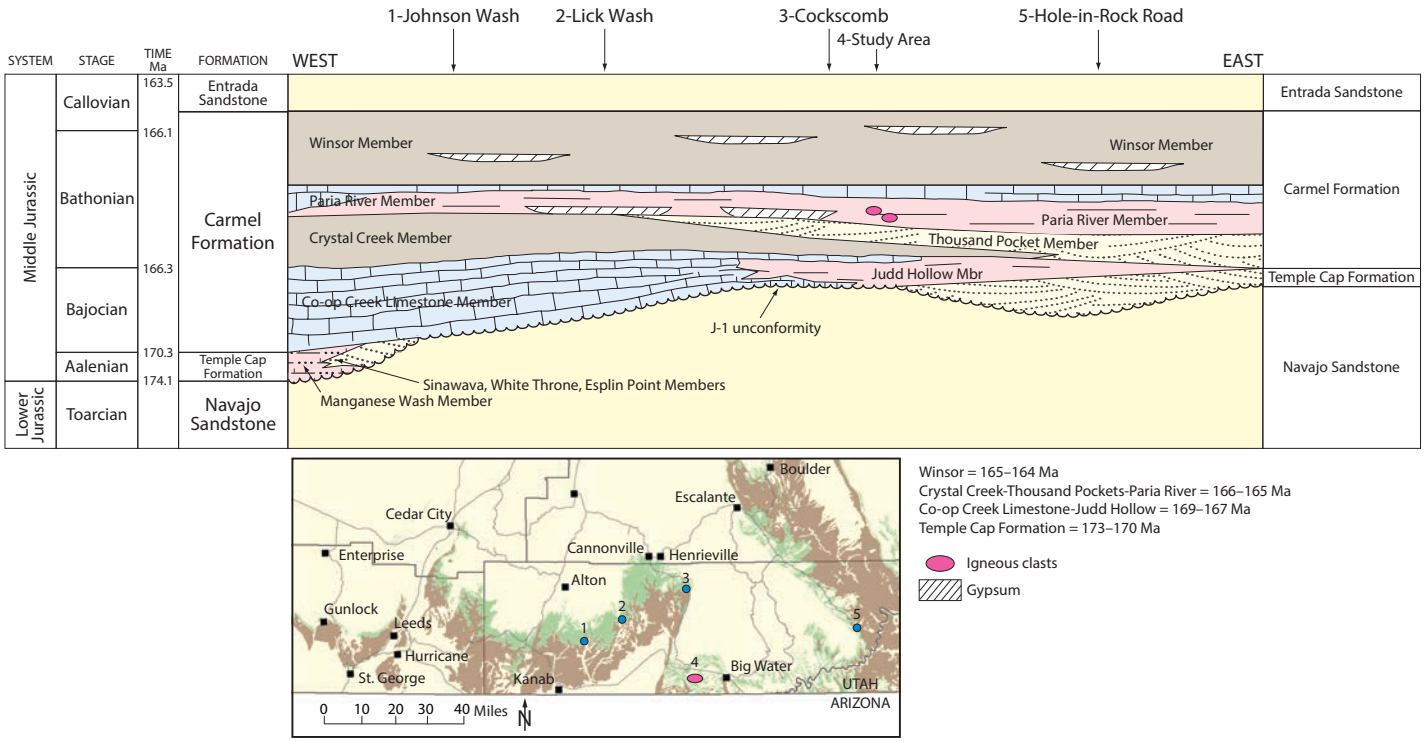

Figure 2. Southwest-to-northeast diagram of formation and member names recommended across the Middle Jurassic embayment in south-central Utah. The Co-op Creek Limestone Member should only be used in southwestern Utah where the member is greater than 25 m thick and where it is mostly limestone in composition. The Carmel Formation east of the Green and Colorado Rivers (not shown on figure) consists of a lower, mostly planar-bedded sandstone unit (for which we will propose the name Rone Bailey Member in a future publication) and an upper, mostly siltstone and mudstone of the established Dewey Bridge Member. An influx of sand from the south is responsible for the sandy nature of the Carmel Formation in the Kaiparowits Basin and the deposition of the Thousand Pockets Member.

170.5 ± 0.95 Ma, which indicate the Temple Cap is Aalenian (Kowallis and others, 2001; Dickinson and others, 2010; Sprinkel and others, 2011; Doelling and others, 2013; Sprinkel and others, in preparation) (figure 3 and table 1).

The Carmel Formation conformably overlies the Temple Cap Formation and contains the igneous clasts; thus, it is described in detail below. Conformably overlying the Carmel Formation is the Entrada Sandstone. The Entrada is exposed about 8 km northwest of the study area and consists mostly of reddish-brown, medium- to large-scale, cross-bedded sandstone that weathers to form rounded bare rock (slickrock) and cliffs (Doelling and others, 1989; Doelling and others, 2010). The Entrada ranges from 90 to 180 m thick in the southern Kaiparowits Basin (Doelling and others, 1989).

Carmel Formation

The Carmel Formation was described and mapped by pioneering geologists investigating the geology of the Kaiparowits area (Gregory and Moore, 1931), the nearby San Rafael Swell (Gilluly and Reeside, 1928), and elsewhere in southern and eastern Utah (Baker and others, 1936). The Carmel is formally subdivided into four members throughout southern Utah with varying names for the lowest two members, which reflect significant lithofacies changes across the region (figure 2). The four members of the Carmel Formation in the Kaiparowits Basin include (in stratigraphic ascending order) the Judd Hollow, Thousand Pockets-Crystal Creek, Paria River, and Winsor Members (figure 2; Phoenix, 1963; Thompson and Stokes, 1970; Blakey and others, 1983; Doelling and others, 1989, 2013). The Carmel

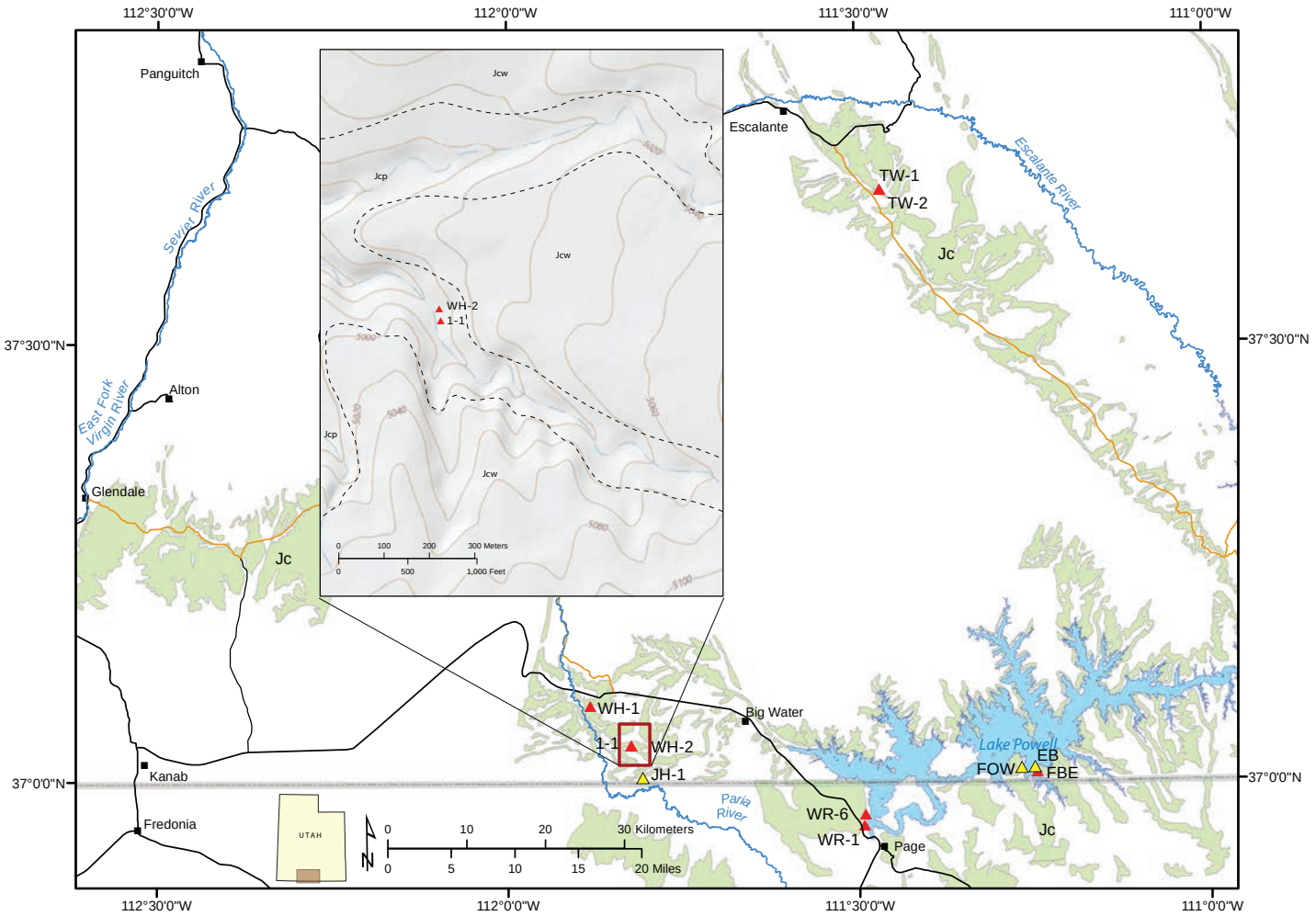

Figure 3. Locations and sample numbers of fallout tuffs with isotopic ages from the Temple Cap (yellow triangles) and Carmel (red triangles) Formations. The Carmel Formation outcrop belt is shown in green (Jc). The inset map shows the locations of the igneous clast collected from the Paria River Member of the Carmel Formation. Jcp – Paria River Member and Jcw – Winsor Member of the Carmel Formation. Results of isotopic age analyses are in table 1.

Formation in this area was deposited near the southern end of a Jurassic Western Interior seaway that occupied nearly all of Utah (Blakey and others, 1983; Brenner, 1983; Kocurek and Dott, 1983). The depositional setting ranges from shallow marine to marginal marine, eolian, and fluvial environments. These members are identifiable by their lithology throughout southwestern and eastern Utah.

The basal member, the Judd Hollow, is dominated by dark to medium reddish-brown sandstone and siltstone beds of marine to marginal marine origin deposited on a tidal flat. The clastic beds of the Judd Hollow Member grade laterally westward to mostly thick marine limestone strata, interbedded with thin marginal marine sandstone and mudstone beds of the correlative Co-op Creek Limestone Member (Doelling and others, 1989; Doelling and others, 2013). Palynomorphs recovered from the mudstone beds and isotopic ages of 169.0 ± 0.62 to 168.2 ± 1.3 Ma (concordant U-Pb zircon) from ash beds indicate the Judd Hollow is Bajocian in age (Sprinkel and others, 2011; Doelling and others, 2013; Sprinkel and others, in preparation) (figure 3 and table 1). These ages are consistent with the palynologic and isotopic ages obtained from the Co-op Creek Limestone Member (Kowallis and others, 2001; Sprinkel and others, 2011; Sprinkel and others, in preparation). The

Table 1. Sample locations and radiometric ages.

Sample Number	Field Number	Type of Sample	Latitude	Longitude	(± 2σ)	Mineral Dated
1-1	PH-2015-05-15-1-1	Cobble-sized clast	37.041537	-111.824346	171.73 ± 0.19	Ar/Ar sanidine
1-2	PH-2015-05-15-1-2	Cobble-sized clast	37.041550	-111.824321		
1-3	PH-2015-05-15-1-3	Cobble-sized clast	37.041687	-111.824493		
1-4	PH-2015-05-15-1-4	Cobble-sized clast	37.041687	-111.824493		
1-5	PH-2015-05-15-1-5	Cobble-sized clast	37.041687	-111.824493		
2-1	PH-2015-05-15-2-1	Boulder-sized clast	37.041687	-111.824493		
WH-1	WH-07-20-2013-1	Fallout tuff	37.087886	-111.882425	163.6 ± 3.3	U-Pb zircon
WH-2	WH-07-20-2013-2	Cobble-sized clast	37.041766	-111.824458	174 ± 5	U-Pb zircon
WR-1	WR-111808-1	Fallout tuff	36.950250	-111.492433	164.40 ±4.50	Ar/Ar sanidine
WR-6	WR-111808-6	Fallout tuff	36.962217	-111.490983	167.10 ±0.70	Ar/Ar sanidine
JH-1	JH-111708-1	Sandstone	37.004900	-111.808200	170.5 ±0.95	U-Pb zircon
EB	East Bay	Fallout tuff	37.015167	-111.249817	171.02 ±0.92	Ar/Ar biotite
FBE	Face Bay East	Fallout tuff	37.009567	-111.245800	169.52 ±0.99	Ar/Ar biotite
FOW	Face One West	Fallout tuff	37.014333	-111.268450	171.90 ±1.9	U-Pb zircon
TW-1	TW-111908-1	Sandstone	37.645417	-111.464393	168.20 ± 1.30	U-Pb zircon
TW-2	TW-111908-2	Fallout tuff	37.645958	-111.465062	165.30 ± 1.20	U-Pb zircon
NOM	GR-051809-1A	Fallout tuff	38.680934	-110.154717	167.68 ± 0.82	U-Pb zircon
NOM	RC-051909-2	Fallout tuff	38.752650	-110.038550	166.70 ± 0.52	U-Pb zircon

Note: Locations are also shown on figure 3 except 2 sample marked as NOM = locations not on map. Samples 1-1, 1-2, 1-3, 1-4, and 2-1 all come from the locality and are labeled as 1-1 on figure 3.

Judd Hollow Member thins eastward from 17 m in the study area to 8 m near Lake Powell (Peterson and Pipiringos, 1979; Wright and others, 1979; Doelling and others, 1989).

The overlying Thousand Pockets Member of the Carmel Formation (Doelling and others, 2013) is dominated by eolian sand. The unit generally intertongues with fine-grained, marginal marine (tidal flat) red beds of the Crystal Creek Member (Peterson and Pipiringos, 1979; Doelling and others, 2013). Fallout tuff beds are preserved in several sections of the Crystal Creek Member within and outside of the study area. Outside of the study area ages of 166.0 ± 0.7 to 165.0 ± 1.2 Ma (U-Pb zircon; Sprinkel and others, 2011; Doelling and others, 2013; Sprinkel and others, in preparation) have been reported (figure 3 and table 1). An age of 167.1 ± 0.7 Ma (2σ, sanidine $^{40}Ar/^{39}Ar$) comes from a sample collected at the top of the Thousand Pockets or the base of the overlying Paria River Member. In the study area, the Thousand Pockets and intertonguing Crystal Creek Members are about 60 to 85 m thick and thin eastward near Lake Powell to about 38 m thick (Peterson and Pipiringos, 1979; Wright and others, 1979; Doelling and others, 1989).

The Paria River Member overlies the Thousand Pockets-Crystal Creek Members and consists generally of dark reddish-brown to light-gray sandstone of marginal marine to fluvial origin deposited mostly on a tidal flat. Some sandstone beds are mottled or banded with shades of light- to dark-brown, light-gray, and purplish-gray hues. The Paria River includes interbedded dark reddish-brown siltstone and thin beds of dark reddish-brown mudstone and thin beds of calcarenite to limestone. The unit also contains several conglomerate beds, which are of interest because they contain the ignimbrite clasts. The description, chemistry, and age

of the igneous clasts are discussed in a separate section as they are the focus of this study. Regionally, the Paria River Member ranges from about 80 to 180 m thick and thins eastward to 15 m near Lake Powell (Peterson and Pipiringos, 1979; Wright and others, 1979; Doelling and others, 1989). Within the study area, the Paria River Member is 20 to 23 m thick (Wheatley, 2018) (figure 4).

The capping Winsor Member of the Carmel Formation consists of interbedded sandstone, siltstone, and silty mudstone of marginal marine to fluvial origin deposited on a tidal flat. The Winsor strata are varicolored forming a colorful banded unit that ranges from dark reddish-brown, reddish-orange, pale-orange, and light-brown to grayish purple, greenish-gray, and light-gray beds. Gypsum beds are typically found in the Winsor Member but are notably absent in the study area. Also atypical in the study area is the amount of sandy material that has infiltrated the member. The sandy nature of the Winsor is likely related to the same source of sand that is responsible for deposition of the Thousand Pockets Member (Doelling and others, 2013). A volcanic ash bed sampled from near the base of the Winsor Member (figure 3 and table 1) in the study area provided a U-Pb zircon age of 163.6 ± 3.3 Ma (U-Pb zircon) and indicates a Callovian age. Palynomorphs recovered from mudstone beds outside the study area indicate that the Winsor Member is Bathonian to Callovian (Sprinkel and others, 2011; Sprinkel and others, in preparation). The Winsor Member ranges from about 95 to 110 m in the general study area but thins eastward to about 78 m near Lake Powell.

METHODS

Samples of volcanic cobbles and of possible volcanic ash were collected in 2013 and 2015 from the Carmel Formation east of Kanab (table 1 and figure 3). The outcrop consists of a layer that contains mostly volcanic pebbles and cobbles in various stages of preservation (figure 5). We collected several of the best-preserved clasts (clasts 1-1, 1-2, 1-3, 1-4, and 1-5), in addition to a sample of a large, highly-weathered volcanic boulder (2-1) that was at least 0.5 m across (we could not determine its full size because it was partially buried). Two of us (Sprinkel and Wheatley) earlier collected material from a purplish-gray, weathered clast (WH-2) out of the same conglomeratic layer from which we collected the other clasts. In addition, we collected a biotite-rich, purple, altered, and likely reworked, fallout tuff (WH-1) from near the White House campground on the Paria River approximately 1 m above the base of the Winsor Member. The cobbles were cut to a billet from which polished thin sections were produced for petrographic and electron microprobe analysis (table 2).

A split of each sample was first washed in acid to remove carbonate cement and areas where carbonate has replaced the original tuff. After drying, the split was then pulverized in a tungsten carbide shatter box or agate ball mill for whole-rock chemical analysis. X-ray fluorescence (XRF) analyses were done at Brigham Young University using a Siemens SRS-303 spectrometer. Major elements (Si, Al, Ti, Fe, Mn, Mg, Ca, Na, K, and P) were determined on glass disks formed by fusing rock powder with lithium metaborate and are reported as oxides. Trace elements (Ba, Ce, Cr, Cu, Ga, La, Nb, Nd, Ni, Pb, Rb, Sc, Sm, Sr, Th, U, V, Y, Zn, and Zr) were determined on pressed powder pellets with a cellulose backing (table 3). In both cases, natural rocks were used as calibration standards. Analytical precision and accuracy were assessed from repeat analyses of international geochemical reference materials.

Clast 1-1 contained an abundance of clear, apparently unaltered sanidine crystals and a piece of this clast was sent to the WiscAr Geochronology Laboratory at the University of Wisconsin-Madison for mineral separation $^{40}Ar/^{39}Ar$ dating. The $^{40}Ar/^{39}Ar$ ages were calculated relative to the FC-201 sanidine standard age of 28.201 Ma and a total ^{40}K decay constant of 5.643 e-10/a (Kuiper and others, 2008). Methodology for laser fusion dating of single crystals of sanidine is outlined on the WiscAr Lab website (https://geochronology.geoscience.wisc.edu/analytical-approaches/), and values used in calculations are given in table 4 along with data on individual grains. Zircons were extracted by heavy-liquid separation methods from the possible fallout tuff (WH-1) and from a cobble-sized clast (WH-2). Laser ablation ICP-MS spot analyses were collected in zircon grains by Apatite to Zircon, Inc. Their analytical methodology is available upon request to the authors.

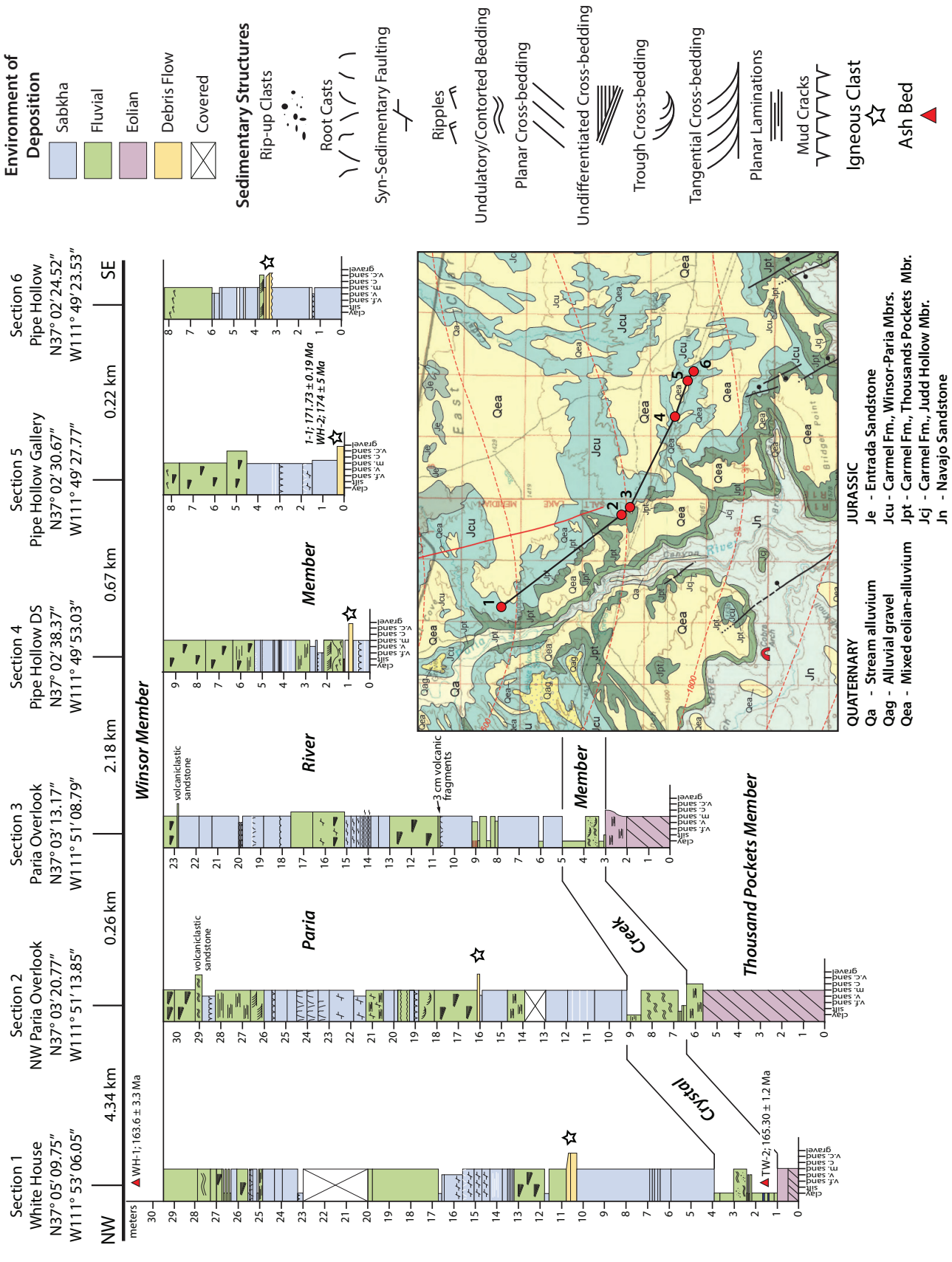

Figure 4. Measured sections of the Paria River Member of the Carmel Formation in the Paria Canyon area showing the beds that contain the igneous clasts. These beds are interpreted as debris-flow deposits. Samples WH-1 and WH-2 (see table 1) were collected from near measured section 4. Modified from Wheatley and Chan (2018). Geologic map from Doeliing and Willis (2006). Structure contours (red dashed lines) drawn at base of the Naturita Formation (formerly Dakota Formation). Contour interval is 100 m.

Figure 5. (top) Large, rounded igneous, boulder-sized clast from the White House area (37.089487, -111.885517) near sample WH-1. The boulder has broken into several large pieces having maximum diameters of 1.3, 1.0, and 0.8 m with several other 0.5 m blocks and is compositionally similar to other igneous clasts in the area. (Photo credit: Mark Hansford). (bottom) Layer with volcanic cobbles where samples 1-1 through 1-5 were collected (see table 1 for location).

CHARACTER OF THE CLASTS

Petrography: Phenocrysts, Textures, and Welding

Chapman (1987, 1989, 1993) characterized a large number of clasts from these deposits and concluded that almost all of the large clasts (>1 cm) were welded rhyolite tuffs. In the clasts smaller than about 1 cm, some were of intermediate and mafic composition, as well as intrusive igneous rocks, and a few metamorphic rocks. Our focus was not to duplicate Chapman's efforts, but to better characterize the rhyolite tuff clasts that comprise the majority of the clasts within the conglomerates and all of the larger cobbles and boulders.

Thin section examination of the rhyolite clasts reveals that most of them have nicely preserved relict shard textures (figures 6 and 7). Shards are not flattened and only weakly oriented preferentially in most of the samples, preserving round bubble walls and bubble triple junctions (figures 6A, 6B, and 7C). Relict pumice fragments are also not significantly flattened (figure 7). Figure 7D shows several slightly flattened pumices, but in figure 7C the large relict pumice is fairly equant. Our examination of these thin sections shows that the tuffs were not significantly welded, and must have had fairly low rock densities at the time of transportation and deposition.

Phenocrysts preserved in the clasts include sanidine, quartz, biotite, apatite, and zircon. Sanidine grains are preserved with little or no alteration in some of these volcanic clasts. They appear as clear euhedral to subhedral grains in thin section (figures 6A, 6E, 6F, 6H, and 7B,). Quartz is frequently embayed (figures 6E and 6F), suggesting that it was being resorbed at the time of eruption. Biotite occurs as partially to completely oxidized booklets (figure 6G). Dark oxides are concentrated on cleavage planes where fluids could alter them. Plagioclase is not preserved, but must have initially been present in the tuffs as noted for other tuffs from the Temple Cap and Carmel Formations (Kowallis and others, 2001). Relict amphibole appears as iron oxides surrounding calcite cores (figures 6C and 6D) and relict pumice fragments as fine-grained aggregates of quartz and feldspar (figure 7B). Thin sections from sample WH-2 have less abundant quartz and sanidine, more abundant relict pumice, and fewer relict amphiboles. No primary Fe-Ti oxides appear to have survived in any of the samples. Nonetheless, the mineral assemblage is consistent with a rhyolitic bulk composition.

XRF analyses (figure 8 and table 2) also show the rocks were probably rhyolites and trachytes before alteration. However, their K_2O contents are anomalously high (6.5 to almost 8% in the fresher clasts and over 10% in the altered boulder), and Na_2O values are low (0.8 to 1.3% in the fresher clasts and 0% in the altered boulder), when compared to fresh rhyolite, indicating that secondary alteration has significantly modified their chemistry. CaO concentrations (0.13 to 0.02 wt%) are

Table 2. Selected electron microprobe analyses of sanidine and biotite.

Sample Number	Analysis Number	SiO_2	TiO_2	Al_2O_3	FeO	MnO	MgO	CaO	BaO	Na_2O	K_2O	F	Cl	SUM	H_2O*	Total
Sanidine																
1-1	6b	66.17		18.94	0.19			0.25	0.07	4.12	11.03					100.76
1-1	6c	66.47		18.94	0.16			0.23	0.21	4.24	11.01					101.26
1-2	10c	66.07		19.03	0.14			0.24	0.62	4.30	10.55					100.95
1-2	10d	65.88		18.97	0.17			0.22	0.52	4.39	10.82					100.97
1-3	2-8	65.72		18.79	0.17			0.27	0.50	4.16	10.88					100.48
1-3	2-9	66.00		18.42	0.18			0.28	0.34	4.05	10.96					100.23
1-4	5d	65.57		19.01	0.08			0.36	0.39	4.29	10.94					100.64
1-4	5e	65.68		19.11	0.18			0.26	0.47	4.05	11.11					100.87
1-5	3-2	65.08		18.92	0.08			0.21	0.80	3.00	12.50					100.59
1-5	3-3	65.28		18.52	0.08			0.17	0.66	3.04	12.60					100.35
WH-2	b-1c	63.41		19.25	0.17			0.26	2.41	3.60	11.47					100.56
WH-2	b-3b	63.90		19.04	0.19			0.29	1.78	3.66	11.60					100.45
Biotite																
1-1	2a	37.69	4.21	13.35	15.42	0.60	15.41	0.00	0.33	0.60	9.51	1.28	0.18	97.99	3.33	101.32
1-1	2b	37.78	4.37	13.19	15.31	0.61	15.11	0.01	0.22	0.60	9.43	1.31	0.20	97.53	3.28	100.81
1-2	5a	36.81	4.19	12.38	12.74	1.63	18.56	0.03	0.17	0.57	9.35	4.48	0.16	99.14	1.87	101.01
1-2	5b	37.26	4.35	13.03	13.08	1.31	17.53	0.01	0.17	0.68	9.62	4.01	0.17	99.48	2.08	101.56
1-3	3b	36.91	4.28	12.93	15.74	0.55	15.03	0.03	0.36	0.62	9.49	1.70	0.18	97.05	3.06	100.11
1-3	3c	37.73	4.31	12.81	15.68	0.55	15.17	0.02	0.09	0.59	9.67	1.58	0.16	97.66	3.16	100.82
1-4	1c	36.61	4.21	13.11	13.63	1.16	16.93	0.03	0.49	0.57	9.38	4.07	0.18	98.62	2.00	100.62
1-4	2a	35.73	4.13	13.24	13.50	1.45	17.74	0.06	0.60	0.52	9.04	4.16	0.15	98.54	1.99	100.53
1-5	2c	36.22	4.58	13.60	19.52	0.29	12.85	0.00	0.17	0.50	9.47	1.12	0.24	98.02	3.32	101.34
1-5	3a	36.48	4.55	13.49	18.16	0.28	12.98	0.00	0.24	0.28	9.62	2.21	0.26	97.56	2.76	100.32
WH-2	2-a8	35.28	5.19	14.56	15.93	0.45	14.23	0.00	2.39	0.54	9.06	1.00	0.05	98.25	3.42	101.67
WH-2	3-a12	34.36	5.55	14.21	16.13	0.49	13.49	0.00	2.69	0.55	8.55	0.92	0.07	96.60	3.37	99.97

*Calculated value for water in biotite

also lower than the 0.5 wt% typically found in rhyolite. Immobile element concentrations can be used to infer the probable original volcanic rock types before alteration (see for example, Christiansen and others, 2015).

On tectonic discrimination diagrams (figure 9) using Nb versus Y, most of the samples plot in the volcanic arc field (Pearce, 1996) and are similar to analyses from the Temple Cap and Carmel Formations published previously (Kowallis and others, 2001).

We also collected electron microprobe analyses from biotite and feldspar in the clasts (table 3). Only sanidine feldspar grains are preserved in the tuff clasts. This preservation is like that found in altered fallout tuff beds from the Carmel and Temple Cap Formations (Kowallis and others, 2001). The composition of sanidine grains falls into three groups (figure 10). Clast 1-5 is distinctive with the highest Or content (Or_{72}–Or_{76}). WH-2 sanidine is also distinctive, but has lower Or values (Or_{64}–Or_{69}). All the other clasts clump between Or_{59} and Or_{64}. The same three groups appear on a plot of K versus Ba in these sanidines (figure 11). WH-2 grains have the highest Ba content and are typically unzoned in Ba (one grain out of six that were probed had a rim with lower Ba content). Clast 1-5 is also distinctive with high K and intermediate Ba concentrations. All of the sanidine in the other clasts clump together.

Biotite occurs in all of the ignimbrite clasts we examined. Compositions of biotite in terms of molar Fe/(Fe + Mg) and total Al relative to ideal end members

Table 3. X-ray fluorescence analyses (major and trace elements) for Carmel Formation clasts.

Sample Number	1-1	1-2	1-3	1-4	1-5	2-1	2-2	2-3
Major Elements (wt%)								
SiO_2	74.44	72.83	73.79	77.71	76.50	62.69	63.25	62.60
TiO_2	0.16	0.16	0.24	0.16	0.32	0.35	0.35	0.35
Al_2O_3	12.80	13.76	12.49	10.90	10.39	18.23	18.55	19.01
Fe_2O_3	1.93	2.04	2.53	1.73	3.05	3.65	3.46	3.42
MnO	0.03	0.03	0.03	0.06	0.02	0.02	0.02	0.01
MgO	0.12	0.18	0.20	0.10	0.22	0.42	0.45	0.40
CaO	0.12	0.13	0.07	0.11	0.12	0.02	0.01	0.01
Na_2O	1.25	1.31	0.84	1.14	0.88	0.00	0.00	0.00
K_2O	6.45	6.65	7.87	7.21	7.06	10.11	10.31	10.47
P_2O_5	0.01	0.01	0.02	0.00	0.01	0.02	0.01	0.01
LOI	2.08	2.09	1.26	0.64	0.72	4.40	3.73	3.78
TOTAL	99.38	99.19	99.33	99.76	99.29	99.90	100.15	100.06
Trace Elements (ppm)								
Ba	383	364	589	751	591	324	275	297
Ce	18	20	141	7	23	75	68	64
Cr	0	0	1	1	16	1	1	0
Cu	5	4	3	4	7	18	4	6
Ga	12	12	10	9	8	18	18	18
La	11	12	40	5	12	29	23	24
Nb	13	13	17	12	16	21	20	21
Nd	10	12	61	3	7	34	30	29
Ni	3	2	2	1	2	2	2	3
Pb	9	11	14	9	15	8	8	8
Rb	173	175	191	168	208	146	145	151
Sc	1	2	1	0	1	4	4	4
Sm	4	3	10	2	3	6	6	5
Sr	25	23	38	40	47	20	17	15
Th	14	17	19	13	24	19	19	17
U	3	4	4	4	5	4	4	4
V	14	15	32	12	37	24	20	24
Y	26	25	34	7	21	39	36	33
Zn	20	19	10	14	12	32	19	21
Zr	131	123	190	139	181	250	244	244

fall mostly within the field for calc-alkaline igneous rocks from the western United States (Christiansen and others, 1986; figure 12a), with sample 1-5 bordering on the lower end of the field for the rhyolitic Bishop Tuff, and similar to the composition of the dacitic Fish Canyon Tuff (Hildreth, 1979; Whitney and Stormer, 1985; Christiansen and others, 1986). The low Fe/Mg ratios of the biotite indicate a high oxygen fugacity and are thus consistent with generation in a subduction-related magmatic arc. Fluorine content of biotite from these tuffs is also similar to that of the Fish Canyon Tuff but only slightly overlaps into the field for biotite from other Middle Jurassic tuff beds in the Temple Cap and Carmel Formations that we have previously examined (Kowallis and others, 2001; figure 12b). A number of grains from samples 1-2 and 1-4 plot at higher F and Mg content than the rest of the grains, suggesting that they have been affected by secondary alteration; these anomalous grains also have low Al_{tot} (figure 12a).

Based on the biotite and feldspar compositions, it appears that the cobble and boulder deposits in the Carmel Formation have clasts from a minimum of three different volcanic units. Because our sampling of clasts was fairly limited, it is likely that the actual number of different eruptive units is higher.

In conclusion, the volcanic clasts in this part of the Carmel Formation appear to be rhyolite ignimbrites, in agreement with Chapman's (1987, 1989, 1993) original assessment of the clasts. However, we disagree with Chapman on the degree of welding. Chapman (1987) stated that the clasts are "partly welded to welded rhyolitic tuff" and that the "boulders of welded tuff could not have been derived from the distal non-welded edges of an ignimbrite sheet" (Chapman, 1993). Smith (1960) examined welding in ash flow tuffs and stated, "The degree of welding may range from incipient stages marked by the sticking together or cohesion of glassy fragments at their points of contact and within the softening range of the glass to complete welding marked by the cohesion of the surfaces of glassy fragments accompanied by their deformation and the elimination of pore space." Smith (1960) continued by saying that, "deformation of pumiceous fragments and shards is the only positive criterion of welding in the tuffs which have crystallized, particularly in older rocks." Using these criteria, we propose that the clasts were derived from the non-welded to incipiently welded parts of an ignimbrite sheet; none of the clasts we examined showed evidence of strong welding. Welded rhyolite tuffs have rock densities of 1.8 to 2.4 g/cm^3, whereas poorly to non-welded rhyolite tuffs have densities of 1.0 to 1.8 g/ cm^3 (Healey, 1970; Olsson,

Table 4. Complete $^{40}Ar/^{39}Ar$ results for sample 1-1 relative to 28.201 Ma for the Fish Canyon sanidine standard.

Sample: PH-2015-05-15-1
J-value: 0.0076692 ± 0.0000038 (1σ)
D/amu: 1.00844 ± 0.00081 (1σ)
Material: sanidine

File	Laser Power (%)	^{40}Ar (moles)	^{40}Ar (Volts)	± 1σ^{40} (Volts)	^{39}Ar (Volts)	±1σ^{39} (Volts)	^{38}Ar (Volts)	± 1σ^{38} (Volts)	^{37}Ar (Volts)	± 1σ^{37} (Volts)	^{36}Ar (Volts)	± 1σ^{36} (Volts)	%$^{40}Ar^*$	$^{40}Ar^*/^{39}ArK$	± 1σ	Age ± 2σ (Ma) (Ma)	K/Ca	Included in wtd. mean
MAA6559-000	35	4.961E-14	8.406077	0.003547	0.653555	0.000810	0.007948	0.000069	0.007986	0.000227	0.000063	0.000006	99.78	12.834015	0.01705	171.84 ± 0.44	35.188	✓
MAA6560-000	35	4.366E-14	7.397286	0.002444	0.574471	0.000575	0.006884	0.000069	0.006729	0.000203	0.000157	0.000006	99.37	12.795578	0.01384	171.35 ± 0.35	36.711	✓
MAA6562-000	35	3.984E-14	6.750625	0.001703	0.523307	0.000549	0.006443	0.000083	0.006144	0.000163	0.000138	0.000006	99.39	12.821501	0.01426	171.68 ± 0.36	36.623	✓
MAA6563-000	35	2.555E-14	4.328882	0.001103	0.336589	0.000369	0.003921	0.000068	0.003593	0.000120	0.000047	0.000005	99.67	12.819297	0.01522	171.66 ± 0.39	40.280	✓
MAA6565-000	35	4.842E-14	8.204402	0.003231	0.639151	0.000685	0.007647	0.000096	0.007106	0.000219	0.000045	0.000006	99.84	12.815712	0.01488	171.61 ± 0.38	38.674	✓
MAA6566-000	35	2.851E-14	4.830154	0.001200	0.372299	0.000399	0.004346	0.000058	0.004061	0.000138	0.000178	0.000006	98.90	12.831667	0.01493	171.81 ± 0.38	39.421	✓
MAA6568-000	35	3.577E-14	6.060312	0.002578	0.468278	0.000591	0.005611	0.000107	0.006166	0.000176	0.000088	0.000006	99.57	12.886439	0.01757	172.51 ± 0.45	32.654	
MAA6569-000	35	4.387E-14	7.433803	0.002655	0.575598	0.000725	0.006895	0.000063	0.007401	0.000232	0.000149	0.000006	99.41	12.838286	0.01709	171.90 ± 0.44	33.442	✓
MAA6572-000	35	3.366E-14	5.703067	0.002595	0.443905	0.000507	0.005203	0.000072	0.005078	0.000183	0.000041	0.000006	99.79	12.820249	0.01620	171.67 ± 0.41	37.593	✓
MAA6574-000	35	3.844E-14	6.513183	0.001594	0.506706	0.000641	0.006028	0.000047	0.006152	0.000170	0.000075	0.000006	99.66	12.810434	0.01686	171.54 ± 0.43	35.417	✓
MAA6575-000	35	2.984E-14	5.056347	0.001547	0.393671	0.000433	0.004611	0.000077	0.004389	0.000157	0.000035	0.000006	99.79	12.817781	0.01522	171.64 ± 0.39	38.567	✓
MAA6577-000	35	2.870E-14	4.863305	0.001598	0.377742	0.000388	0.004519	0.000039	0.004432	0.000126	0.000027	0.000006	99.84	12.853864	0.01456	172.10 ± 0.37	36.653	✓
MAA6578-000	35	6.103E-14	10.340820	0.003301	0.803746	0.000804	0.009523	0.000070	0.009783	0.000318	0.000095	0.000006	99.73	12.831062	0.01369	171.81 ± 0.35	35.328	✓
MAA6580-000	35	2.007E-14	3.401186	0.001073	0.265214	0.000318	0.003221	0.000059	0.003187	0.000132	0.000036	0.000006	99.69	12.784545	0.01708	171.21 ± 0.44	35.780	✓
MAA6581-000	35	3.003E-14	5.087868	0.002012	0.395552	0.000518	0.004749	0.000052	0.006915	0.000195	0.000048	0.000006	99.73	12.827476	0.01804	171.76 ± 0.46	24.596	✓
MAA6583-000	35	2.722E-14	4.611322	0.001312	0.358535	0.000377	0.004203	0.000035	0.004062	0.000162	0.000051	0.000006	99.67	12.819626	0.01473	171.66 ± 0.38	37.953	✓
MAA6584-000	35	3.655E-14	6.192323	0.002086	0.481534	0.000552	0.005803	0.000089	0.020370	0.000478	0.000229	0.000006	98.92	12.720702	0.01572	170.40 ± 0.40	10.165	
MAA6586-000	35	3.682E-14	6.238065	0.002662	0.481407	0.000542	0.005740	0.000080	0.005666	0.000228	0.000069	0.000006	99.67	12.915916	0.01597	172.89 ± 0.41	36.532	
MAA6587-000	35	4.488E-14	7.603898	0.002230	0.589959	0.000652	0.007106	0.000110	0.006937	0.000185	0.000097	0.000006	99.62	12.840243	0.01496	171.92 ± 0.38	36.571	✓
MAA6589-000	35	3.326E-14	5.635394	0.001135	0.437354	0.000486	0.005324	0.000070	0.005070	0.000185	0.000062	0.000006	99.67	12.843179	0.01507	171.96 ± 0.39	37.091	✓
MAA6590-000	35	2.899E-14	4.911342	0.002850	0.381940	0.000499	0.004559	0.000055	0.004048	0.000155	0.000032	0.000006	99.81	12.834454	0.01886	171.85 ± 0.48	40.569	✓
MAA6593-000	35	2.345E-14	3.972390	0.001441	0.308118	0.000365	0.003641	0.000033	0.003528	0.000137	0.000055	0.000006	99.59	12.839651	0.01684	171.92 ± 0.43	37.558	✓
MAA6595-000	35	2.869E-14	4.860277	0.001356	0.378092	0.000475	0.004418	0.000040	0.004128	0.000143	0.000046	0.000006	99.72	12.818761	0.01705	171.65 ± 0.44	39.386	✓
														weighted mean age (20 of 23):		171.73 ± 0.19		

The values in this table represent blank, discrimination, and decay (^{37}Ar and ^{39}Ar) corrected values.

Atmospheric argon ratios		
$^{40}Ar/^{36}Ar$	298.56 ± 0.31	Lee and others (2006)
$^{38}Ar/^{36}Ar$	0.1885 ± 0.0003	Lee and others (2006)

Decay constants		
λ_{40Ar}	(0.580 ± 0.014) x 10-10 a-1	Min and others (2000)
λ_{B-}	(4.884 ± 0.099) x 10-10 a-1	Min and others (2000)
^{39}Ar	(2.58 ± 0.03) x 10-3 a-1	Stoenner and others (1965)
^{37}Ar	(8.23 ± 0.042) x 10-4 h-1	Stoenner and others (1965)
^{36}Cl	(2.303 ± 0.046) x 10-6 a-1	

Interfering isotope production ratios	
$(^{40}Ar/^{39}Ar)K$	(5.4 ± 1.4) x 10^{-4}
$(^{38}Ar/^{39}Ar)K$	(1.210 ± 0.002) x 10^{-2}
$(^{39}Ar/^{37}Ar)Ca$	(6.95 ± 0.09) x 10^{-4}
$(^{38}Ar/^{37}Ar)Ca$	(1.96 ± 0.08) x 10^{-5}
$(^{36}Ar/^{37}Ar)Ca$	(2.65 ± 0.022) x 10^{-4}

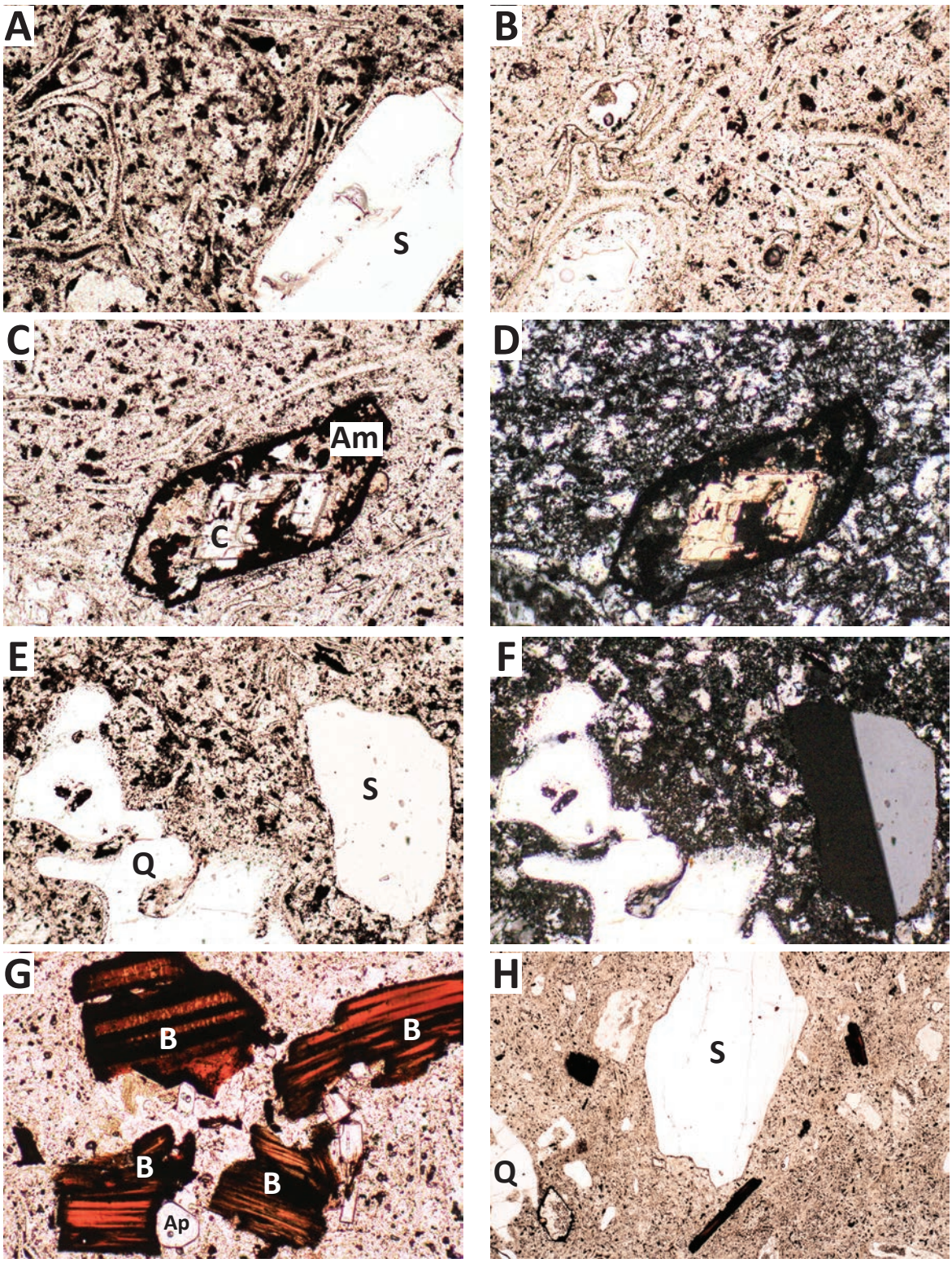

Figure 6. Textures and minerals in the clasts. Clast 1-1 shown in A, E, F, and G; clast 1-2 in B, C, and D; clast 1-4 in H. The wide dimension on all the photomicrographs is about 1 mm, except for photomicrograph H, which is 5 mm. S = sanidine, Q = quartz, C = calcite, B = biotite, Am = relict amphibole, Ap = apatite. Pairs C-D and E-F are plane and cross-polarized images of the same area. All other photomicrographs are in plane-polarized light.

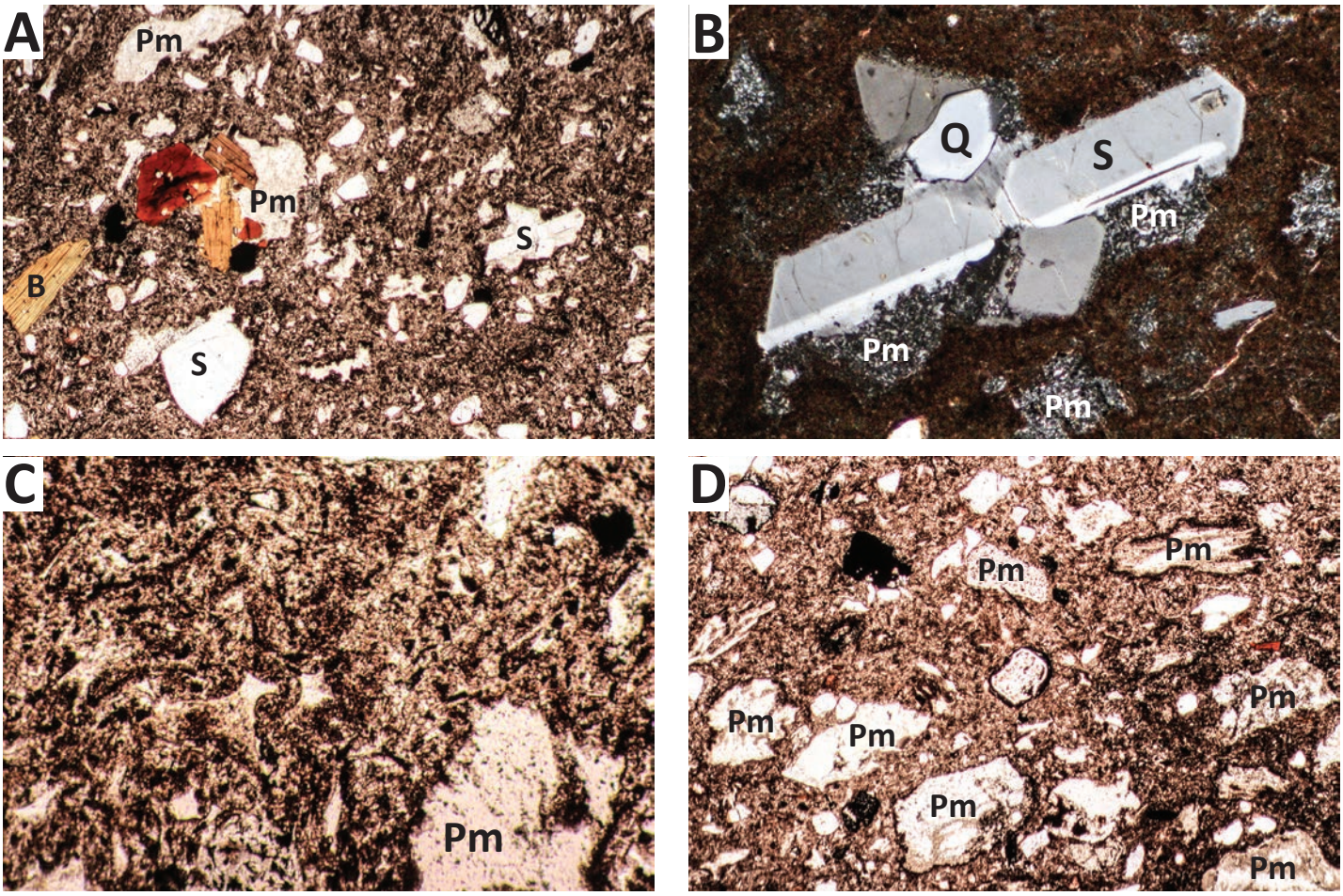

Figure 7. Textures and minerals in clast WH-2. The wide dimension on all the photomicrographs is about 5 mm, except for photo B, which is 1 mm. S = sanidine, Q = quartz, C = calcite, B = biotite, Pm = pumice. Photomicrographs A, C, and D are plane-polarized light. Photomicrograph B is a blow-up of part of A taken in cross-polarized light.

1991; Wohletz and Heiken, 1992). Moving low-density, non-welded tuff boulders over long distances would be much easier than moving blocks of more densely welded tuff, but they would also be more friable.

Age

Chapman (1993) reported a $^{40}Ar/^{39}Ar$ age of 169 ± 4 Ma for one clast provided only as an oral communication from John Obradovich at the U.S. Geological Survey (this age would be ~171 Ma using current decay constants and standards).

The age of the Carmel Formation sediments enclosing the volcanic clast layer can be estimated from the age of fallout tuff sample WH-1, which gave a TuffZirc age of 163.6 +3.3/-1.4 Ma for a group of 45 coherent grains and a U-Pb weighted mean age of 163.9 ± ~3.3 Ma (figure 13; assuming a 2% error, 2-sigma, [see Gehrels and others, 2008]). This age fits well with other ages (~162–164 Ma) obtained from the upper part of the Carmel Formation by palynology and radiometric dating of other ash beds (table 1; Sprinkel and others, 2011). No zircons older than the Middle Jurassic were identified. On the other hand, zircons from tuff clast WH-2 gave a spectrum of ages ranging from Middle Jurassic to Archean even though it lacks any evidence of a sedimentary component. A TuffZirc analysis of the youngest grains from WH-2 produced a coherent group of 20 grains with an age of 174 ± ~5 Ma (figure 14). This age is significantly older than other ages we have obtained from the volcanic deposits in the upper members

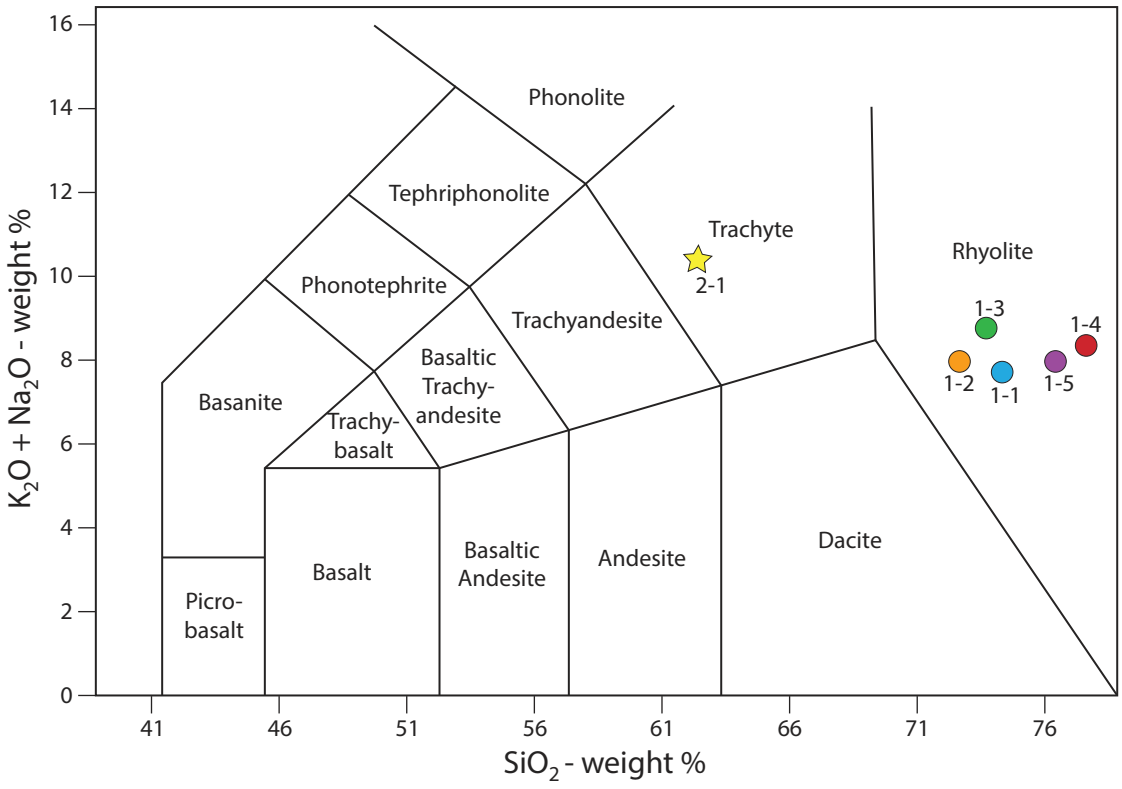

Figure 8. Total alkali versus silica volcanic rock classification diagram (after Le Bas and others, 1986). Sample numbers are shown next to data points.

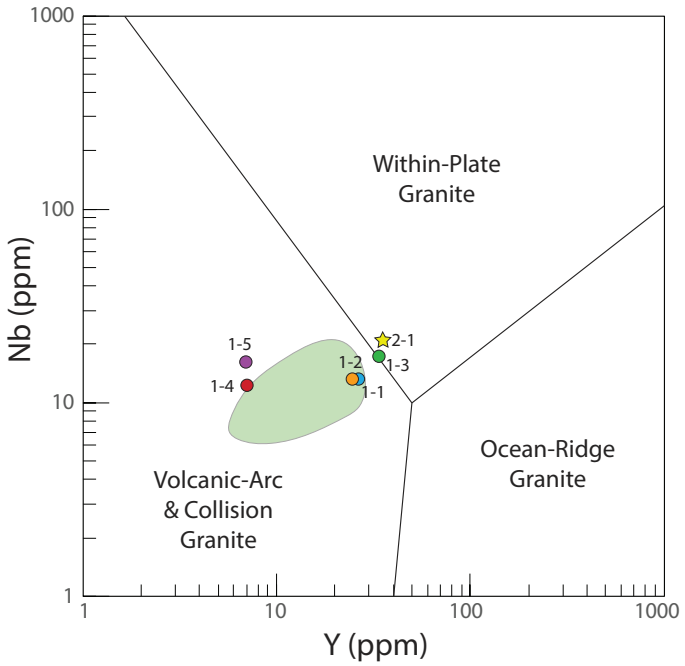

Figure 9. Nb and Y trace element compositions of volcanic clasts from the Carmel Formation fall in the volcanic arc field on the discriminant diagram of Pearce and others (1984). The green area compares the clast compositions to those of ash beds in the Carmel and Temple Cap Formations from Kowallis and others (2001).

of the Carmel Formation (Sprinkel and others, 2011) and seems likely to represent the age of the youngest detritus in this sample. The older detrital grains in sample WH-2 match up well with the signal obtained from Lower and Middle Jurassic strata of the Colorado Plateau by Dickinson and Gehrels (2010).

Sanidine grains have been preserved with little or no alteration in some of the volcanic clasts. They appear as clear euhedral to subhedral grains in thin section (figures 6A, 6E, 6H, and 7B). A laser-fusion, single-crystal $^{40}Ar/^{39}Ar$ age of 171.73 ± 0.19 Ma was obtained on sanidine from clast 1-1 (figure 15 and table 4). This age is similar to ages obtained by Kowallis and others (2001) from sanidine from fallout tuffs in the Temple Cap Formation in southwestern Utah (ages ranging from 170.24 to 172.93 ± ~0.5 to 0.6 Ma; corrected to new Fish Canyon age standard and decay constants following Kuiper and others [2008]). Dickinson and others (2010) dated a tuff from an eolianite equivalent to the Temple Cap Formation collected farther east in southernmost Utah along the shores of Lake Powell (see figure 1 in Dickinson and others, 2010). Their sample gave a U-Pb zircon age of 171.5 to 171.9 ± ~2.0 Ma and an $^{40}Ar/^{39}Ar$ biotite

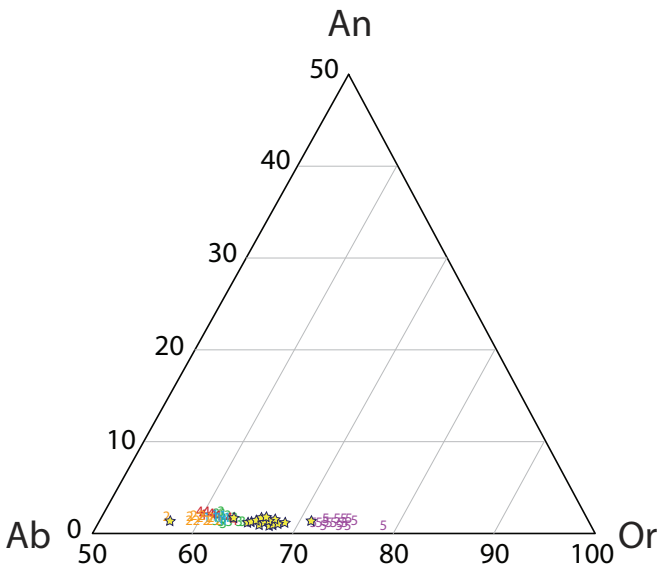

Figure 10. Compositions of sanidine grains from the clasts collected at sites PH-2015-05-15 (samples 1-1 to 1-5) and WH-07-20-2013-2 (WH-2 stars).

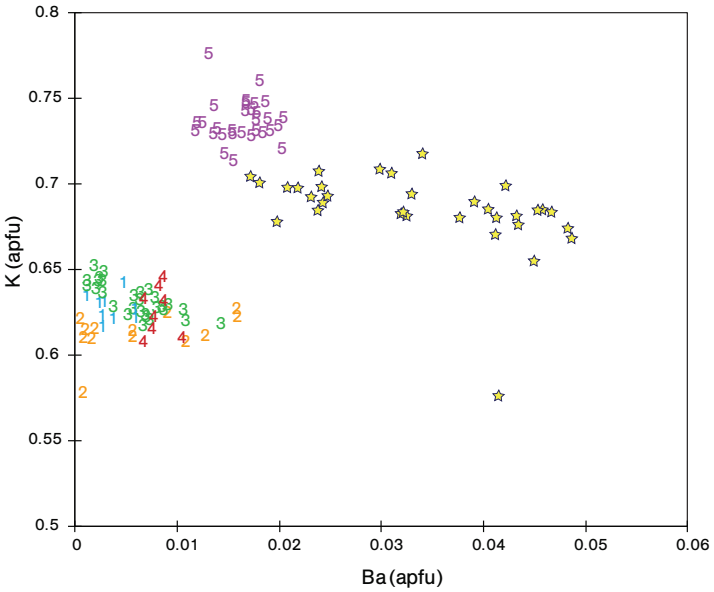

Figure 11. Barium (Ba) concentration in sanidine grains (atoms per formula unit) plotted versus K from clasts collected at sites PH-2015-05-15 (samples 1-1 to 1-5) and WH-07-20-2013-2 (WH-2 stars).

age of 171.02 ± 0.92 Ma.

Our new ages, along with the earlier age reported in Chapman (1993), provide clear evidence that the clasts in the conglomerates found in the upper Carmel Formation are derived from outcrops of volcanic rocks of Temple Cap Formation age that are approximately 8 to 10 million years older than the Carmel Formation deposit in which they are found.

MOVING BOULDERS ACROSS A LARGE DISTANCE

Nearest Outcrops

The nearest current outcrops of Middle Jurassic volcanic rocks of the right age (~170 Ma) are located in the lower Colorado River region of southern California and southwestern Arizona (Tosdal and Wooden, 2015). Chapman (1987) proposed that the magmatic arc was closer during the Jurassic than it is today due to Basin and Range extension in order to account for transporting coarse volcanic boulders and cobbles ~350 km (straight line, closest current distance) from the Jurassic arc to the depositional site in south-central Utah (figure 16). However, because a significant portion of the distance between the arc and the deposit falls on the Colorado Plateau (~180 km), which was not extended, how much shortening can we reasonably propose for the remaining 170 km? Estimates of horizontal extension due to Basin and Range activity vary widely from extremes of 400% to as little as 20% (Hintze and Kowallis, 2009). Extension near the latitude of Las Vegas, Nevada, in an area called the Colorado River extensional corridor has been the subject of several papers. Wernicke and others (1988) proposed extension in this region of 300 to 400%. Faulds and others (1990, 2001) discuss the extension in this region but do not give a percentage, only stating that large amounts of extension occurred. Marzolf (1990), in general agreement with Wernicke and others (1988), produced a Middle Jurassic palinspastic reconstruction of the southwestern United States showing a significant reduction (225 km as opposed to 350 km) in the distance the boulders would need to travel from a proposed tuff apron around the arc (figure 16). Two-hundred and twenty-five km is still a substantial distance over which to move large boulders.

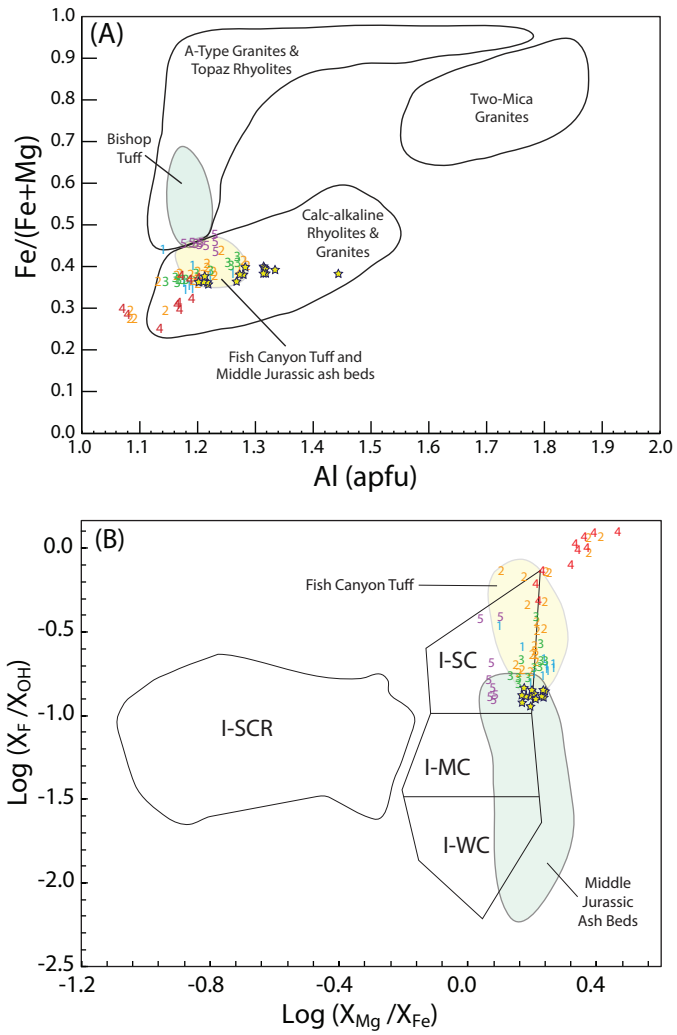

Figure 12. (A) Compositions of biotite from Carmel Formation clasts compared to Fish Canyon and Bishop Tuffs (Hildreth, 1979) in terms of molar Fe/(Fe + Mg) and total Al relative to ideal end member. Fields for different types of granite are from Christiansen and others (1986). (B) Compositions of biotite from Carmel Formation clasts compared to biotite from the Fish Canyon Tuff and Middle Jurassic ash beds from Temple Cap and Carmel Formations (Kowallis and others, 2001). Granite fields from Ague and Brimhall (1988): I-SCR = I-type, strongly contaminated and reduced; I-SC = I-type, strongly contaminated; I-MC = I-type, moderately contaminated; I-WC = I-type, weakly contaminated.

Run-out Distances for Tuffs

Chapman (1987) also suggested that a factor to consider was the run-out distance for ash-flow tuffs and compiled a list of 17 eruptions where the run-out was over 30 km; two of them, a member of the Bates Mountain Tuff (now called the Nine Hill Tuff) and the Peach Springs Tuff, perhaps exceeded 200 km of run-out. We have compiled a larger list of 48 ignimbrites from the Cenozoic of the western United States with maximum run-outs greater than 40 km (corrected for post-eruption extension, table 5). Of these tuffs, 22 have maximum run-outs of over 100 km, and 5 have run-outs of 200 km or more. The Nine Hill Tuff provides an informative comparison. Henry and Faulds (2009) showed that this tuff was channeled in river valleys that cut across the (then lower) Sierra Nevada batholith from its eruptive source in western Nevada—a distance of over 200 km when corrected for later extension. These paleovalleys are typically 7 to 10 km wide and as much as 1 km deep. If the Carmel Formation cobbles and boulders were sourced from distal run-out lobes where flow was extended because of focusing in paleovalleys, then the distance from the tuff outcrops to the conglomerate depositional site could be reduced by another 100 to 200 km. As discussed earlier in this paper, our analysis of the clasts shows them to be poorly welded to unwelded, not unusual for distal parts of an ignimbrite.

If we use the palinspastically reconstructed distance proposed by Marzolf (1990) of about 225 km and the run-out distances from table 5, then distal outflow ignimbrites could have been deposited close to the location of the gravel and boulder beds of the Paria River Member of the Carmel Formation.

Remobilizing the Outcrops as Debris Flows

Based upon careful analysis of the sedimentology of the clast-bearing outcrops, Chapman (1987, 1993) concluded that these deposits were formed from debris flows or lahars that likely occurred shortly after eruption, with the tuffs being laid down on a softer substrate of quartz-rich sedimentary rock (Chapman, 1989). We agree that the clast-bearing deposits represent one or more debris flows but disagree that these flows occurred soon after eruption of the tuffs. The ages on the clasts range between 171 and 174 Ma, whereas the age of the enclosing Paria River Member is ~163 to 167 Ma (table 1 and figure 4; Doelling and others, 2013), 5 to 10 Ma younger. Regardless of the age of the clasts, they were incorporated into a debris-flow rich in volcanic detritus

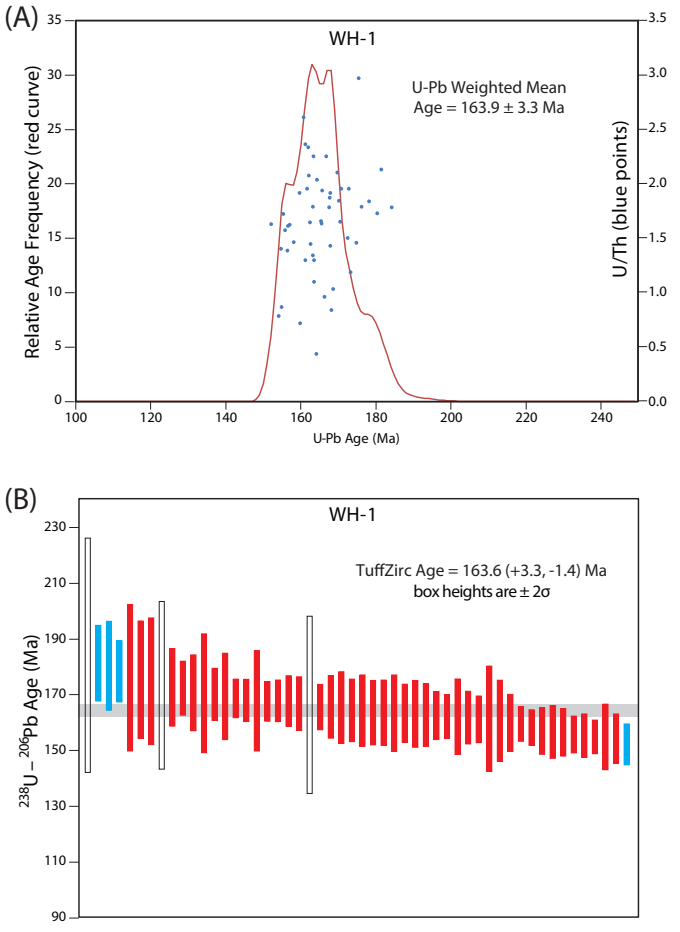

Figure 13. 238U-206Pb ages for zircons from the basal Winsor Member of the Carmel Formation ash bed WH-1. (A) A relative age probability diagram of individual U-Pb grain ages (red curve) (Hurford and others, 1984, and Kowallis and others, 1986). Also shown are U/Th ratios (blue dots) for each analyzed spot. (B) TuffZirc plot (Ludwig and Mundil, 2002) for zircons from sample WH-1. Blue bars and open bars are analyses not included in the overall age. The blue bars do not overlap the error range and the open bars are low resolution ages.

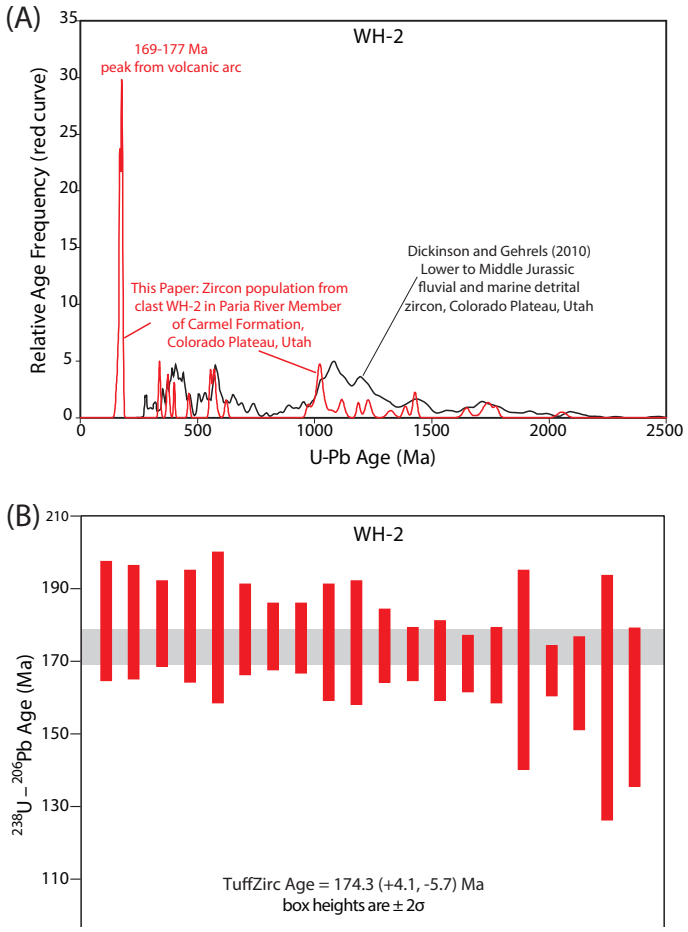

Figure 14. (A) ^{238}U-^{206}Pb zircon ages from sample WH-2 (red line) plotted with the detrital zircon ages reported by Dickinson and Gehrels (2010) from Lower to Middle Jurassic sedimentary rocks of the Colorado Plateau. The peaks from both curves correlate quite well neglecting the young population of grains in WH-2. (B) U-Pb TuffZirc plot for the subset of young zircons from clast WH-2.

that must have been sourced in an area where multiple volcanic tuffs had accumulated on a surface with a significant east or northeast slope.

Debris flows are capable of transporting very large clasts and may travel distances in excess of 100 km (Neall, 1976; Siebert and others, 1987; Carrasco-Núñez and others, 1993; Mothes and others, 1998; Scott and others, 2001). However, they are typically sourced in fairly steep terrain. As an example, Mothes and others (1998) stated that, "The Chillos Valley Lahar (CVL), the largest Holocene debris flow in area and volume as yet recognized in the northern Andes, formed on Cotopaxi volcano's north and northeast slopes and descended river systems that took it 326 km north–northwest to the Pacific Ocean and 130+ km east into the Amazon basin." More recently, the eruption of Nevado del Ruiz volcano in Colombia in 1985 produced lahars that traveled 60 to 70 km from their source along the channels of the

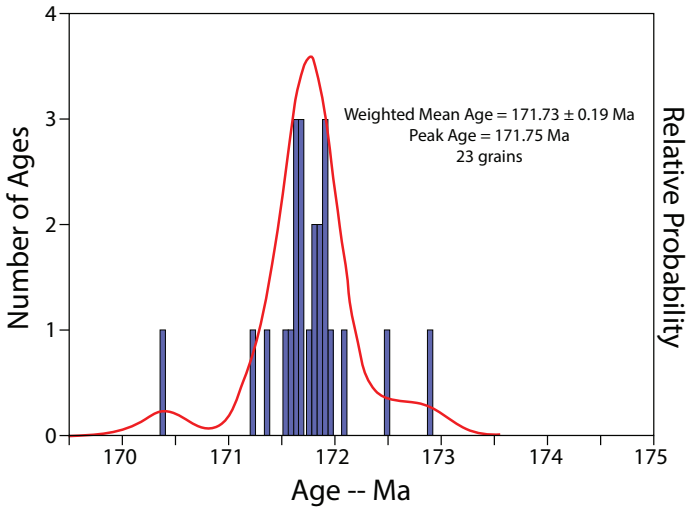

Figure 15. Relative probability plot for $^{40}Ar/^{39}Ar$ sanidine ages from clast 1-1. Bars are individual grain ages.

Rio Azufrado and Rio Lagunillas, burying the city of Armero and killing more than 25,000 people (Naranjo and others, 1986; Voight, 1990).

To provide the necessary slope for debris flows to form and transport the clasts, we propose that the distal tuff deposits described above were deposited in a highland area northeast of the low-standing Middle Jurassic arc. They remained in place for several million years after their initial emplacement during which time they were subjected to weathering and alteration. Even poorly welded tuffs would likely be more resistant to erosion than the silt and mud of the underlying Temple Cap-age sediments. As erosion and weathering progressed, it is possible that inverted valley topography formed (Cundari and Ollier, 1970; Hamblin, 1987) with the tuffs rising somewhat above the surrounding country, providing additional gravitational potential and the slope needed for moving the clasts by debris flows over the last few tens of kilometers to reach the depositional site. In southwestern Utah, basaltic lavas have produced inverted topography of over 300 m relief in less than 3 million years (Hamblin, 1987; Biek and others, 2009).

DISCUSSION

The eruptive sources of the large ignimbrite clasts in the Jurassic Carmel Formation of southern Utah remain problematic. Emplacement of the parental ignimbrites occurred in southern California and across southern Nevada and northern Arizona with distal lobes extending up to 200 km from their vents (figure 16). These lobes would have reached across the location of the modern-day Grand Canyon. After remaining in place and weathering for some 5 to 10 million years, they were remobilized as debris flows that carried the clasts the remaining distance (±50 km) into their current depositional setting. This would account for even the large boulder-sized clasts found in the Paria River Member of the Carmel Formation. However, the event or events that brought the clasts into the depositional basin were not common, as we do not find the volcanic clasts throughout the Carmel Formation. Their occurrence is restricted to only one or two horizons. Chapman (1993) proposed that the boulder beds in the Carmel Formation required catastrophic floods to carry the boulders over the transport distance of 200 to 300 km to get them from their source to the depositional site. This proposed flooding could have originated in a highland arc terrain due to excessive rainfall or due to the collapse of a crater lake or natural volcanic dam. Alexander and Cooker (2016) have shown that during flash floods—defined as any overland flow of water within or outside a river channel that arrives suddenly at a fixed point, changes quickly, and lasts a short time—large boulders can be moved farther than would normally be predicted due to the inherently unstable nature of the flow. We agree with Chapman that this type of event could be a possible trigger for the deposits. However, as we have discussed above, the distance required for transport was likely much less than 200 to 300 km and more likely in the range of 50 km. This distance is not unreasonable for a debris flow to carry the low-density tuff boulders and cobbles.

Near an active arc, another possible triggering factor may have been earthquakes. Scott and others (2001) give examples of several earthquake-triggered debris flows, with some traveling over 100 km from their sources. For example, a 1994 earthquake in Colombia generated a debris flow that "conveyed a catastrophic wave of debris" along the Río Páez for over 100 km (Scott and others, 2001). It is apparent that earthquakes large enough to liquefy and deform the sedimentary de-

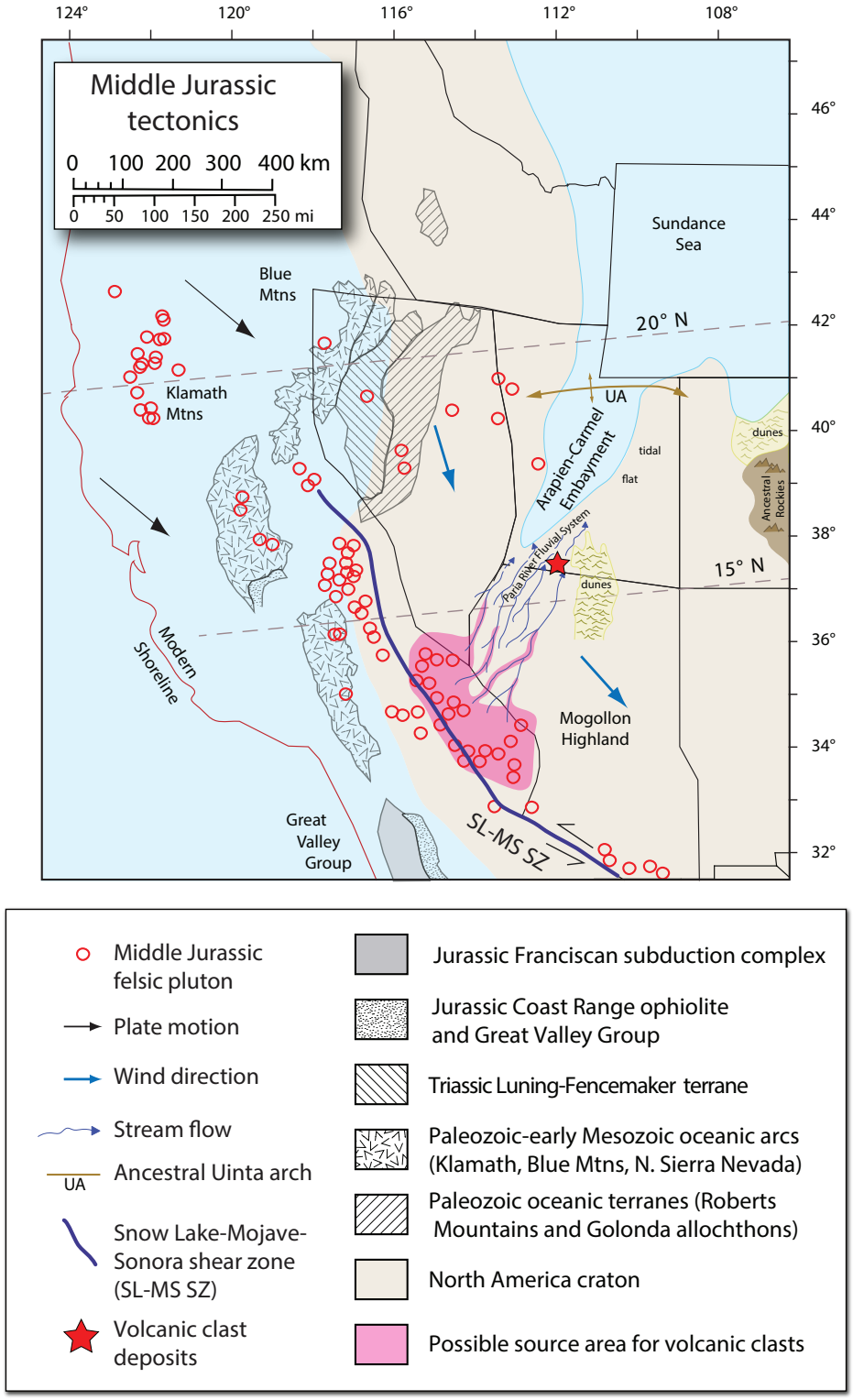

Figure 16. Paleogeographic and tectonic map for the Middle Jurassic during deposition of the Paria River Member of the Carmel Formation. Information used in compiling this figure comes from Blakey and others (1983), Kocurek and Dott (1983), Chapman (1987), Busby-Spera (1988), Thorman and others (1991), Dilek and Moores (1993), Taylor and others (1993), Christiansen and others (1994), Lawton (1994), Marzolf (1994), Peterson (1994), Blakey and Parnell (1995), DeCelles and Currie (1996), Lawton and McMillan (1999), Kowallis and others (2001), and Dickinson (2006).

Table 5. Runout distances for selected ignimbrites from the western United States.

Stratigraphic Unit	Age (Ma)	Composition	Location	Runout (km) Corrected	Correction Factor	Runout (km) Today	Reference
Fraction Tuff	18.6	Rhyolite	Central Nevada VF	44	0.714	62	Best and others, 2013a
Pahranagat Formation	22.9	Rhyolite	Central Nevada VF	114	0.714	160	Best and others, 2013a
Tuff of Clipper Gap	25.0	Rhyolite	Central Nevada VF	214	0.714	300	Best and others, 2013a
Tuff of Lunar Cuesta	25.7	Dacite-rhyolite	Central Nevada VF	130	0.850	153	Best and others, 2013a
Upper Tuff Member of SPF	26.4	Rhyolite	Central Nevada VF	200	1.000	200	Best and others, 2013a
Tikaboo Tuff Member of SPF	26.8	Rhyolite	Central Nevada VF	114	0.850	134	Best and others, 2013a
Hancock Tuff Member of SPF	26.8	Rhyolite	Central Nevada VF	80	0.714	112	Best and others, 2013a
Lower Tuff Member of SPF	27.0	Rhyolite	Central Nevada VF	121	1.000	121	Best and others, 2013a
Tuff of Orange Lichen Creek	27.1	Rhyolite	Central Nevada VF	61	0.850	72	Best and others, 2013a
Monotony Tuff	27.6	Dacite-rhyolite	Central Nevada VF	136	0.850	160	Best and others, 2013a
Tuff of Hot Creek Canyon	30.0	Rhyolite	Central Nevada VF	43	1.000	43	Best and others, 2013a
Windous Butte Formation	31.7	Dacite-rhyolite	Central Nevada VF	228	0.850	268	Best and others, 2013a
Pancake Summit Tuff	35.3	Rhyolite	Central Nevada VF	78	0.850	92	Best and others, 2013a
Stone Cabin Upper Member	35.8	Rhyolite	Central Nevada VF	76	1.000	76	Best and others, 2013a
Stone Cabin Middle Member	35.8	Rhyolite	Central Nevada VF	76	0.850	89	Best and others, 2013a
Hiko	22.6	Rhyolite	Caliente caldera complex	65	0.733	89	Best and others, 2013a
Racer Canyon	18.6	Dacite-rhyolite	Caliente caldera complex	49	1.000	49	Best and others, 2013a
Harmony Hills Tuff	22.6	Andesite	Caliente caldera complex	116	0.870	133	Best and others, 2013a
Bauers Tuff	23.0	Rhyolite	Caliente caldera complex	120	1.000	120	Best and others, 2013a
Swett Tuff	24.2	Rhyolite	Caliente caldera complex	143	0.733	195	Best and others, 2013a
Leach Canyon	24.0	Rhyolite	Caliente caldera complex	120	0.870	138	Best and others, 2013a
Hole in the Wall Member of Isom Fm	24.6	Trachydacite	Indian Peak VF	80	0.666	120	Best and others, 2013a
Bald Hills Member of Isom Fm	27.5	Trachydacite	Indian Peak VF	107	0.666	160	Best and others, 2013a
Ripgut Tuff	29.0	Rhyolite	Indian Peak VF	61	0.870	70	Best and others, 2013a
Petroglyph Cliff Tuff	29.1	Dacite-trachydacite	Indian Peak VF	43	0.870	50	Best and others, 2013a
Lund Tuff	29.2	Dacite	Indian Peak VF	97	0.666	145	Best and others, 2013a
Silver King Tuff	29.4	Dacite-rhyolite	Indian Peak VF	42	0.666	63	Best and others, 2013a
Mackleprang Tuff	30.0	Rhyolite	Indian Peak VF	61	0.666	92	Best and others, 2013a
Greens Cayon	30.1	Rhyolite	Indian Peak VF	19	0.666	29	Best and others, 2013a
Deadman Spring	30.0	Dacite	Indian Peak VF	50	0.870	58	Best and others, 2013a
Wash Wah Springs Tuff	30.1	Dacite	Indian Peak VF	133	0.666	200	Best and others, 2013a
Cottonwood Wash Tuff	31.1	Dacite	Indian Peak VF	104	0.870	120	Best and others, 2013a
Lamerdorf	32.0	Rhyolite	Indian Peak VF	64	0.733	87	Best and others, 2013a
Marsden	33.0	Rhyolite	Indian Peak VF	48	0.870	55	Best and others, 2013a
Sawtooth	33.5	Rhyolite	Indian Peak VF	40	1.000	40	Best and others, 2013a
Tunnel Spring Tuff	35.3	Rhyolite	Indian Peak VF	15	0.666	22	Best and others, 2013a
The Gouge Eye	36.0	Dacite-rhyolite	Indian Peak VF	25	1.000	25	Best and others, 2013a
Blue Sphinx/Hu Pwi	24.5	Rhyolite	Western Nevada VF	76	0.870	88	Henry and John, 2013
Bates Mtn A/Rattlesnake Canyon	31.2	Rhyolite	Western Nevada VF	126	0.666	189	Henry and John, 2013
Arc Dome	25.1	Rhyolite	Western Nevada VF	61	0.666	91	Henry and John, 2013
Campbell Creek/Bates Mtn C	28.9	Rhyolite	Western Nevada VF	257	0.733	350	Henry and John, 2013
Candelaria Hills	26.0	Rhyolite	Western Nevada VF	47	0.980	48	Henry and John, 2013
Gabs Valley	25.1	Rhyolite	Western Nevada VF	123	0.733	168	Henry and John, 2013
Nine Hill Tuff	25.4	Rhyolite	Western Nevada VF	167	0.666	250	Henry and John, 2013
New Pass Tuff	25.3	Rhyolite	Western Nevada VF	97	0.666	146	Henry and John, 2013
Singatse Tuff	26.9	Rhyolite	Western Nevada VF	136	0.733	185	Henry and John, 2013
Toiyabe Tuff	23.3	Rhyolite	Western Nevada VF	157	0.733	214	Henry and John, 2013
Mickey Pass Tuff	27.1	Rhyolite	Western Nevada VF	210	0.733	287	Henry and John, 2013

Notes: Corrected for 50% post volcanic east-west extension in western Nevada and central Nevada volcanic fields (VF); corrected for 40% post volcanic east-west extension in Indian Peak volcanic field and Caliente caldera complex; distances in red are for runouts over 100 km; SFP = Shingle Pass Formation.

posits of the Carmel Formation did occur during deposition of this formation. Marzolf (1988, 1990) noted that associated with these boulder and cobble beds in the Carmel Formation are "massive silty sandstones [that] display abundant evidence of liquefaction and fluidization, including remnants of contorted stratification, foundered conglomerate beds, and spectacular elutriation pipes." More recently, Wheatley and others (2016) also concluded that these structures and pipes were likely caused by one or more earthquakes. An earthquake at the right time of year when the source outcrops were saturated with seasonal rainfall or snowmelt could have provided a trigger for the debris flows.

Whatever the triggering mechanism, a highland area to the southwest of the depositional site was needed. From the time of eruption of the tuff beds at about 172 to 174 Ma until the formation of the transporting debris flows, subduction and volcanic activity appear to have been fairly continuous along the Jurassic arc as evidenced by the numerous fallout ash beds that were deposited in the Carmel-Twin Creek (Sundance) seaway (Marvin and others, 1965; Everett and others, 1989; Zhang, 1996; Kowallis and others, 2001; Sprinkel and others, 2011). Busby-Spera (1988) proposed that the arc during this time period was a low-standing, arc-graben. Chapman (1993) countered, arguing that by the time the debris flows were carrying boulders over long distances into the Carmel basin, there must have been a significant highland to the southwest of the depositional site. We agree that debris flows require a significant gravitational potential in order to travel even a few tens of kilometers and that the source area must have been at a significantly higher elevation than the deposits, but this may not necessitate a change in the model of a low-standing arc-graben at the time these deposits were formed. The modern Central American volcanic arc formed along the Middle American trench is in part a low-standing arc-graben similar to what Busby-Spera (1988) proposed for the Middle Jurassic. Figure 17 shows the Central American arc with a low-standing, arc-graben formed between northern Costa Rica and northern Nicaragua. To the northeast of this part of the arc is a highland region with rivers flowing off of it toward the Caribbean coast. We have superimposed on the figure our modeled source area and location of the clast deposits from figure 16. The scale of the modern arc and distance from the arc to the eastern fluvial plain are remarkably similar to what we propose for the Middle Jurassic. Additionally, studies of landslides and debris flows in the highland areas of Guatemala, El Salvador, Costa Rica, and Nicaragua have documented run-out distances of up to 50 km (Alvarado and others, 2004; Siebert and others, 2006; Devoli and others, 2007, 2009), similar to what we propose would have been needed to transport the Middle Jurassic clasts from the outcrop area to the depositional site. Triggers for landslides in Nicaragua include earthquakes, volcanic eruptions, and rainfall associated with tropical storms or hurricanes (Devoli and others, 2007).

CONCLUSIONS

The source for coarse volcanic detritus in the Middle Jurassic Carmel Formation of southern Utah has been problematic. We propose that poorly welded rhyolite tuffs generated during Temple Cap Formation time (~173 Ma) from the Middle Jurassic arc in southern California were likely emplaced in distal run-out lobes focused in fluvial valleys, perhaps as much as 200 km from the source vents extending out across the location of the modern Grand Canyon. These tuff outcrops were then stable for several million years as the processes of weathering and alteration proceeded perhaps producing an inverted topography with the tuffs capping mesas above weaker sedimentary units. About 164 Ma, debris flows sourced in these tuff-capped mesas formed and then flowed perhaps 50 km (but possibly even farther) carrying cobbles and some boulders along channels to the depositional site in fluvial channels on a broad tidal flat. Triggers may have been torrential rain, earthquakes, or some combination of these factors.

ACKNOWLEDGMENTS

We acknowledge the assistance of Michael Dorais, David Tingey, Magnolia Serrano-Tomlinson, and David Tomlinson at Brigham Young University for their assistance with electron microprobe and geochemical analyses, Brian Jicha at the WiscAr Lab at the University of Wisconsin for assistance with $^{40}Ar/^{39}Ar$ analyses,

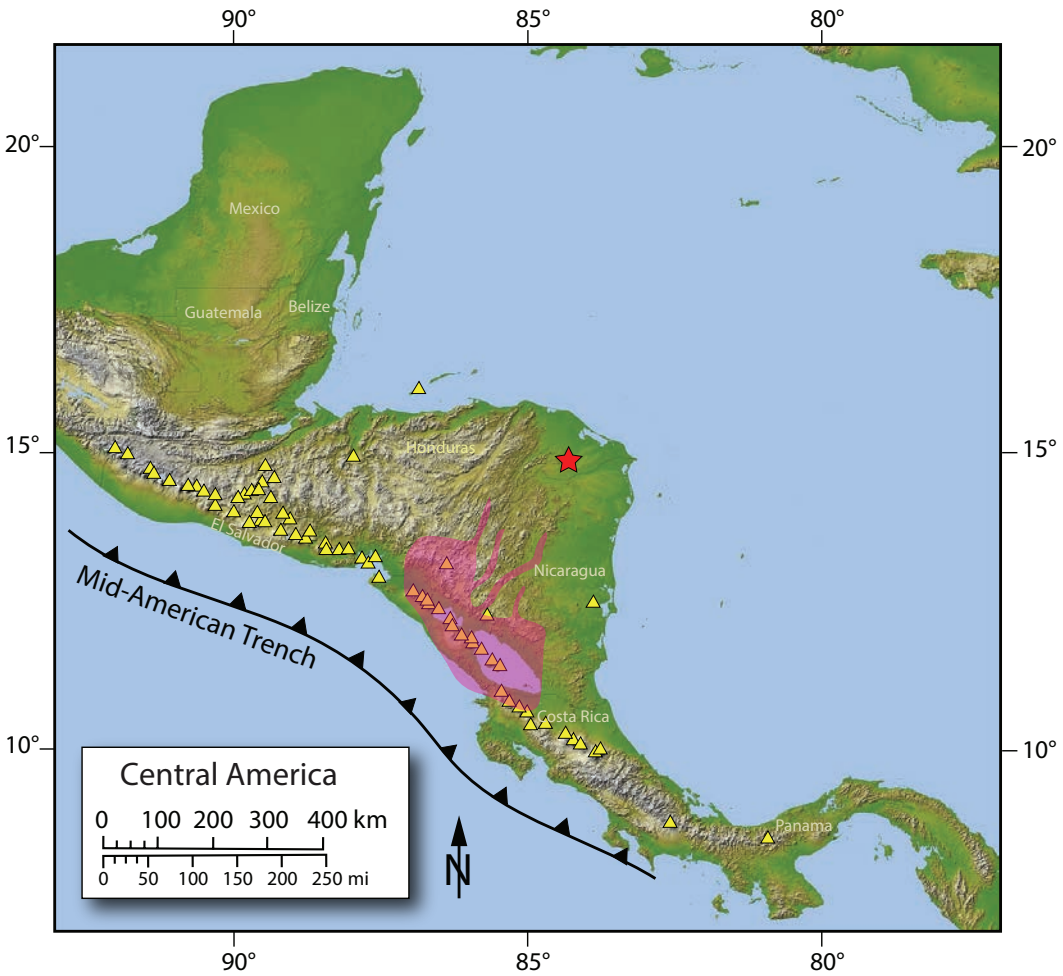

Figure 17. The Central American volcanic arc with the Mid-American trench to the southwest. The pink shaded area is the western U.S. source area shown on figure 16 superimposed over Central America at the same scale; the red star would be the location of the clast deposits. The arc through northern Costa Rica to northern Nicaragua is a low-standing arc-graben. However, highland areas exist to the northeast with rivers flowing off into the Atlantic, similar to what we propose for the time the volcanic clasts were deposited in the Paria River Member of the Carmel Formation. The base map is courtesy of Wikipedia Commons and the volcanoes (yellow triangles) from the Smithsonian Global Program and Alvarado and others (2017).

and Paul O'Sullivan at Apatite to Zircon Inc. for U-Pb analyses. We also thank the Utah Geological Survey and Brigham Young University for financial support for isotopic and geochemical analyses, as well as travel to the field area.

REFERENCES

Ague, J.J., and Brimhall, G.H., 1988, Regional variations in bulk chemistry, mineralogy, and the compositions of mafic and accessory minerals in the batholiths of California: Geological Society of America Bulletin, v. 100, p. 891–911.

Alexander, J., and Cooker, M.J., 2016, Moving boulders in flash floods and estimating flow conditions using boulders in ancient deposits: Sedimentology, v. 63, p. 1582–1595.

Alvarado, G.E., Benito, B., Staller, A., Climent, Á., Camacho, E., Rojas, W., Marroquín, G., Molina, E., Talavera, J.E., Martínez-Cuevas, S., and Lindholm, C., 2017, The new Central American seismic hazard zonation—mutual consensus based on up to day seismotectonic framework: Tectonophysics, v. 721, p. 462–467.

Alvarado, G.E., Vega, E., Chaves, J., and Vásquez, M., 2004, Los grandes deslizamientos (volcánicos y no volcánicos) de tipo debris avalanche en Costa Rica: Revista Geológica de América Central, v. 30, p. 83–99.

Baker, A.A., Dane, C.H., and Reeside, J.B., Jr., 1936, Correlation of the Jurassic formations of parts of Utah, Arizona, New Mexico, and Colorado: U.S. Geological Survey Professional Paper 183, 66 p.

Barth, A.P., Wooden, J.L., Miller, D.M., Howard, K.A., Fox, L.K., Schermer, E.R., and Jacobson, C.E., 2017, Regional and temporal variability of melts during a Cordilleran magma pulse—age and chemical evolution of the Jurassic arc, eastern Mojave Desert, California: Geological Society of America Bulletin, v. 129, p. 429–448, https://doi.org/10.1130/B31550.1.

Best, M.G., Christiansen, E.H, Gromme, S., Deino, A.L., Hart, G., and Tingey, D.G., 2013a, The 36-18 Ma central Nevada ignimbrite field and calderas, Great Basin, USA—multicyclic super eruptions: Geosphere, v. 9, no. 6, p. 1562–1636, https://doi.org/10.1130/GES00945.1.

Best, M.G., Christiansen, E.H, Deino, A.L., Gromme, S., Hart, G., and Tingey, D.G., 2013b, The 36-18 Ma Indian Peak-Caliente ignimbrite field and calderas, southeastern Great Basin, USA—multicyclic super eruptions: Geosphere, v. 9, no. 4, p. 864–950, https://doi.org/10.1130/GES00902.1.

Biek, R.F., Rowley, P.D., Hayden, J.M., Hacker, D.B., Willis, G.C., Hintze, L.F., Anderson, R.E., and Brown, K.D., 2009, Geologic map of the St. George and east part of the Clover Mountains 30' x 60' quadrangles, Washington and Iron Counties, Utah: Utah Geological Survey Map 242, 101 p., 2 plates, scale 1:100,000.

Blakey, R.C., and Parnell, R.A., 1995, Middle Jurassic magmatism—the volcanic record in the eolian Page Sandstone and related Carmel Formation, Colorado Plateau, *in* Miller, D.M., and Busby, C., editors, Jurassic magmatism and tectonics of the North American Cordillera: Geological Society of America Special Paper 299, p. 393–411.

Blakey, R.C., Peterson, F., Caputo, M.V., Geesaman, R.C., and Voorhees, B.J., 1983, Paleogeography of Middle Jurassic continental, shoreline, and shallow marine sedimentation, southern Utah, *in* Reynolds, M.W., and Dolly, E.D., editors, Mesozoic paleogeography of the west-central United States–Rocky Mountain Paleogeography Symposium 2: Rocky Mountain Section SEPM (Society for Sedimentary Geology), p. 77–100.

Brenner, R.L., 1983, Late Jurassic tectonic setting and paleogeography of Western Interior, North America, *in* Reynolds, M.W., and Dolly, E.D., editors, Mesozoic paleogeography of the west-central United States–Rocky Mountain Paleogeography Symposium 2: Rocky Mountain Section SEPM (Society for Sedimentary Geology), p. 119–131.

Busby-Spera, C.J., 1988, Speculative tectonic model for the early Mesozoic arc of the southwest Cordilleran United States: Geology, v. 16, p. 1121–1125.

Busby-Spera, C.J., Mattinson, J.M., Riggs, N.R., and Schermer, E.R., 1990, The Triassic-Jurassic magmatic arc in the Mojave-Sonoran Deserts and the Sierra-Klammath region—similarities and differences in paleogeographic evolution, *in* Harwood, S.S., and Miller, M.M., editors, Paleozoic and early Mesozoic paleogeographic relations—Sierra Nevada, Klammath Mountains, and related terranes: Geological Society of America Special Paper 255, p. 325–337.

Carrasco-Núñez, G, Vallance, J.W., and Rose, W.I., 1993, A voluminous avalanche-induced lahar from Citlaltópetl volcano, Mexico—implications for hazard assessment: Journal of Volcanology and Geothermal Research, v. 59, p. 35–46.

Chapman, M.G., 1987, Depositional and compositional aspects of volcanogenic clast in the upper member of the Carmel Formation, southern Utah: Flagstaff, Northern Arizona University, M.S. thesis, 93 p.

Chapman, M.G., 1989, Implications of rhyolitic ignimbrite boulders in the Middle Jurassic Carmel Formation of southern Utah: Geology, v. 17, p. 281–284.

Chapman, M.G., 1993, Catastrophic floods during the Middle Jurassic—evidence in the upper member and Crystal Creek Member of the Carmel Formation, southern Utah, *in* Dunn, G., and McDougall, K., editors, Mesozoic paleogeography of the western United States II: Denver, Pacific Section SEPM (Society for Sedimentary Geology), book 71, p. 407–416.

Christiansen, E.H, Kowallis, B.J., and Barton, M.D., 1994, Temporal and spatial distribution of volcanic ash in Mesozoic sedimentary rocks of the Western Interior—an alternative record of Mesozoic magmatism, *in* Caputo, M.V., Peterson, J.A., and Franczyk, K.J., editors, Mesozoic systems of the Rocky Mountain region, USA: Denver, Colorado, Rocky Mountain Section SEPM (Society for Sedimentary Geology), p. 73–94.

Christiansen, E.H, Sheridan, M.F., and Burt, D.M., 1986, The Geology and geochemistry of Cenozoic Topaz Rhyolites from the western United States: Geological Society of America Special Paper 205, 82 p.

Christiansen, E.H, Kowallis, B.J., Skidmore, C.N., Pickard, M., and Parks, E., 2015, The record of volcanism in the Brushy Basin Member of the Morrison Formation—implications for the Late Jurassic of western North America: Geological Society of America Special Paper 513, p. 399–439, https://doi.org/10.1130/2015.2513(11).

Cundari, A., and Ollier, C.D., 1970, Inverted relief due to lava flows along valleys: Australia Geographer, v. 11, p. 291–293.

DeCelles, P.G., and Currie, B.S., 1996, Long-term sediment accumulation in the Middle Jurassic–early Eocene Cordilleran retroarc foreland-basin system: Geology, v. 24, p. 591–594.

Devoli, G., De Blasio, F.V., Elverhøi, A., and Høeg, K., 2009, Statistical analysis of landslide events in Central America and their run-out distance: Geotechnical and Geological Engineering, v. 27, p. 23–42.

Devoli, G., Morales, A., and Høeg, K., 2007, Historical landslides in Nicaragua—collection and analysis of data: Landslides, v. 4, p. 5–18.

Dickinson, W.R., 2006, Geotectonic evolution of the Great Basin: Geosphere, v. 2, p. 353–368, https://doi.org/10.1130/GES00054.1.

Dickinson, W.R., and Gehrels, G.E., 2010, Insights into North American paleogeography and paleotectonics from U-Pb ages of detrital zircons in Mesozoic strata of the Colorado Plateau, USA: International Journal of Earth Science, v. 99, p. 1247–1265.

Dickinson, W.R., Stair, K.N., Gehrels, G.E., Peters, L., Kowallis, B.J., Blakey, R.C., Amar, J.R., and Greenhalgh, B.W., 2010, U-Pb and $^{40}Ar/^{39}Ar$ ages for a tephra lens in the Middle Jurassic Page Sandstone—first direct isotopic dating of a Mesozoic eolianite on the Colorado Plateau: The Journal of Geology, v. 118, p. 215–221.

Dilek, Y., and Moores, E.M., 1993, Across-strike anatomy of the Cordilleran orogen at 40° N latitude—implications for the Mesozoic paleogeography of the western United States, *in* Dunn, G., and McDougal, K., editors, Mesozoic paleogeography of the western United States II: Pacific Section SEPM (Society for Sedimentary Geology), book 71, p. 333–346.

Dodge, C.N., 1973, Pebbles from the Chinle and Morrison Formations, *in* James, H.L., editor, Guidebook of Monument Valley and vicinity, Arizona and Utah: New Mexico Geological Society, 24th Field Conference, p. 114–121.

Doelling, H.H., Blackett, R.E., Hamblin, A.H., Powell, J.D., and Pollock, G.L., 2010, Geology of Grand Staircase–Escalante National Monument, *in* Sprinkel, D.A., Chidsey, T.C., Jr., and Anderson, P.B., editors, Geology of Utah's parks and monuments: Utah Geological Association Publication 28 (third edition), p. 193–235.

Doelling, H.H., Davis, F.D., and Brandt, C.J., 1989, The geology of Kane County, Utah—geology, mineral resources, geologic hazards: Utah Geological and Mineral Survey Bulletin 124, 192 p.

Doelling, H.H., Sprinkel, D.A., Kowallis, B.J., and Kuehne, P.A., 2013, Temple Cap and Carmel Formations in the Henry Mountains Basin, Wayne and Garfield Counties, Utah, *in* Morris, T. H., and Ressetar, R., editors, The San Rafael Swell and Henry Mountains Basin—geologic centerpiece of Utah: Utah Geological Association Publication 42, p. 279–318.

Dunne, G.C., 1986, Geologic evolution of the southern Inyo Range, Darwin Plateau, and Argus and Slate Ranges, east-central California—an overview: Cordilleran Section, Geological Society of America Fieldtrip Guidebook, p. 3–21.

Dunne, G.C., and Walker, J.D., 1993, Age of Jurassic volcanism and tectonism, southern Owens Valley region, east-central California: Geological Society of America Bulletin, v. 105, p. 1223–1230.

Everett, B.H., Kowallis, B.J., Christiansen, E.H, and Deino, A., 1989, Correlation of Jurassic sediments of the Carmel and Twin Creek Formations of southern Utah using bentonite characteristics: Utah Geological and Mineral Survey Open-File Report 88-1975, 56 p.

Fackler-Adams, B.N., Busby, C.J., and Mattinson, J.M., 1997, Jurassic magmatism and sedimentation in the Palen Mountains, southeastern California—implications for regional tectonics on the Mesozoic continental arc: Geological Society of America Bulletin, v. 109, no. 11, p. 1464–1484.

Faulds, J.E., Geissman, J.W., and Mawer, C.K., 1990, Structural development of a major extensional accommodation zone in the Basin and Range province, northwestern Arizona and southern Nevada: Geological Society of America Memoir 176, p. 37–76.

Faulds, J.E., Feuerbach, D.L., Miller, C.F., and Smith, E.I., 2001, Cenozoic evolution of the northern Colorado River extensional corridor, southern Nevada and northwest Arizona, *in* Erskine, M.C., Faulds, J.E., Bartley, J.M., and Rowley, P.D., editors, The geologic transition, high plateaus to Great Basin—a symposium and field guide—The Mackin volume: Utah Geological Association Publication 30, Pacific Section American Association of Petroleum Geologists Publication GB78, p. 239–271.

Fohey-Breting, N.K., Barth, A.P., Wooden, J.L., Mazdab, F.K., Carter, C.A., and Schermer, E.R., 2010, Relationship of voluminous ignimbrites to continental arc plutons—petrology of Jurassic ignimbrites and contemporaneous plutons in southern California: Journal of Volcanology and Geothermal Research, v. 189, p. 1–11.

Gehrels, G.E., Valencia, V.A., and Ruiz, J., 2008, Enhanced precision, accuracy, efficiency, and spatial resolution of U-Pb ages by laser ablation–multicollector–inductively coupled plasma–mass spectrometry: Geochemistry, Geophysics, Geosystems, v. 9, no. 3, Q03017, https://doi.org/10.1029/2007GC001805.

Gilluly, J., and Reeside, J.B., Jr., 1928, Sedimentary rocks of the San Rafael Swell and some adjacent areas in eastern Utah: U.S. Geological Survey Professional Paper 150-D, p. D61–D110.

Gregory, H.E., and Moore, R.C., 1931, The Kaiparowits region, a geographic and geologic reconnaissance of parts of Utah and Arizona: U.S. Geological Survey Professional Paper 164, 161 p.

Hamblin, W.K., 1987, Late Cenozoic volcanism in the St. George basin, Utah: Geological Society of America Centennial Field Guide, volume 2–Rocky Mountain Section, p. 291–294.

Healey, D.L., 1970, Calculated in situ bulk densities from subsurface gravity observations and density logs, Nevada Test Site and Hot Creek Valley, Nye County, Nevada: U.S. Geological Survey Professional Paper 700-B, p. B52–B62.

Henry, C.D., and John, D.A., 2013, Magmatism, ash-flow tuffs, and calderas of the ignimbrite flareup in the western Nevada volcanic field, Great Basin, USA: Geosphere, v. 9, p. 951–1008.

Hildreth, E.W., 1979, The Bishop Tuff—evidence for the origin of compositional zonation in silicic magma chambers, *in* Chapin, C.E., and Elston, W.E., editors, Ash-flow tuffs: Geological Society of America Special Paper 180, p. 43–75.

Hintze, L.F., and Kowallis, B.J., 2009, Geologic History of Utah: Brigham Young University Geology Studies, Special Publication 9, 225 p.

Hurford, A.J., Fitch, F.J., and Clarke, A., 1984, Resolution of the age structure of the detrital zircon populations of two Lower Cretaceous sandstones from the Weald of England by fission track dating: Geological Magazine, v. 121, p. 269–277.

Karish, C.R., Miller, E.L., and Sutter, J.F., 1987, Mesozoic tectonic and magmatic history of the central Mojave Desert: Arizona Geological Society Digest, v. 18, p. 15–32.

Kocurek, G., and Dott, R.H., Jr., 1983, Jurassic paleogeography and paleoclimate of the central and southern Rocky Mountains region, *in* Reynolds, M.W., and Dolly, E.D., editors, Mesozoic paleogeography of the west-central United States–Rocky Mountain Paleogeography Symposium 2: Rocky Mountain Section SEPM (Society for Sedimentary Geology), p. 101–116.

Kowallis, B.J., Christiansen, E.H, Deino, A.L., Zhang, C., and Everett, B.H., 2001, The record of Middle Jurassic volcanism in the Carmel and Temple Cap Formations of southwestern Utah: Geological Society of America Bulletin, v. 113, p. 373–387.

Kowallis, B.J., Heaton, J.S., and Bringhurst, 1986, Fission-track dating of volcanically derived sedimentary rocks: Geology, v. 14, p. 19–22.

Kuiper, K.F., Deino, A.L., Hilgen, F.J., Krijgsman, W., Renne, P.R., and Wijbrans, J.R., 2008, Synchronizing the rock clocks of Earth history: Science, v. 320, p. 500–504.

Lawton, T.F., 1994, Tectonic setting of Mesozoic sedimentary basins, Rocky Mountain region, United States, *in* Caputo, M.V., Peterson, J.A., and Franczyk, K.J., editors, Mesozoic systems of the Rocky Mountain region, USA: Rocky Mountain Section SEPM (Society for Sedimentary Geology), p. 1–25.

Lawton, T.F., and McMillan, N.J., 1999, Arc abandonment as a cause for passive continental rifting—comparison of the Jurassic Mexican Borderland rift and the Cenozoic Rio Grande rift: Geology, v. 27, p. 779–782.

Le Bas, M.L., Maitre, R.L., Streckeisen, A., Zanettin, B., and IUGS Subcommission on the Systematics of Igneous Rocks, 1986, A chemical classification of volcanic rocks based on the total alkali-silica diagram: Journal of Petrology, v. 27, p. 745–750.

Lee, J.Y., Marti, K., Severinghaus, J.P., Kawamura, K., Yoo, H.S., Lee, J.B., and Kim, J.S., 2006, A redetermination of the isotopic abundances of atmospheric Ar: Geochimica et Cosmochimica Acta, v. 70, p. 4507–4512.

Ludwig, K.R., and Mundil, R., 2002, Extracting reliable U-Pb ages and errors from complex populations of zircons from Phanerozoic tuffs (Goldschmidt Conference Abstracts 2001): Geochemica Cosmochimica Acta, v. 66, p. A463.

Luscombe, J.E., 2018, Provenance of volcanic clasts within the Paleogene rim gravels, Colorado Plateau—implication for paleogeography and history of the western Grand Canyon: California, San Diego State University, M.S. thesis, 86 p.

Marvin, R.F., Wright, J.C., and Walthall, F.G., 1965, K-Ar and Rb-Sr ages of biotite from the Middle Jurassic part of the Carmel Formation, Utah: U.S. Geological Survey Professional Paper 525-B, p. B104–B107.

Marzolf, J.E., 1988, Reconstruction of Late Triassic and Early and Middle Jurassic sedimentary basins—southwestern Colorado Plateau to the eastern Mojave Desert, *in* Weide, D.L., and Faber, M.L., editors, This extended land—geological journeys in the southern Basin and Range: Geological Society of America Cordilleran Section Field Trip Guidebook, University of Nevada at Las Vegas Geosciences Department Special Publication 2, p. 177–200.

Marzolf, J.E., 1990, Reconstruction of extensionally dismembered early Mesozoic sedimentary basins—southwestern Colorado Plateau to the eastern Mojave Desert: Geological Society of America Memoir 176, p. 477–500.

Marzolf, J.E., 1994, Reconstruction of the early Mesozoic Cordilleran cratonal margin adjacent to the Colorado Plateau, *in* Caputo, M.V., Peterson, J.A., and Franczyk, K.J., editors, Mesozoic systems of the Rocky Mountain region, USA: Denver, Colorado, Rocky Mountain Section SEPM (Society for Sedimentary Geology), p. 181–216.

Min, K., Mundil, R., Renne, P.R., and Ludwig, K.R., 2000, A test for systematic errors in $^{40}Ar/^{39}Ar$ geochronology through comparison with U/Pb analysis of a 1.1-Ga rhyolite: Geochimica et Cosmochimica Acta, v. 64, p.73–98.

Mothes, P.A., Hall, M.L., and Janda, R.J., 1998, The enormous Chillos Valley Lahar—an ash-flow-generated debris flow from Cotopaxi Volcano, Ecuador: Bulletin of Volcanology, v. 59, p. 233–244.

Naranjo, J.L., Sigurdsson, H., Carey, S.N., and Fritz, W., 1986, Eruption of the Nevado Del Ruiz Volcano, Colombia, on 13 November 1985—tephra fall and lahars: Science, v. 233, p. 961–963.

Neall, V.E., 1976, Lahars as major geological hazards: Bulletin of the International Association of Engineering Geology, v. 13, p. 233–240.

Nielson, D.R., 1988, Depositional environments and petrology of the Middle Jurassic Carmel Formation near Gunlock,

Washington County, Utah: Provo, Utah, Brigham Young University, M.S. thesis, 209 p.

Olsson, W.A., 1991, The compressive strength of tuff as a function of strain rate from 10-6 to 103/sec [abs.]: International Journal of Rock Mechanics & Geomechanical Abstracts, v. 28, p. 115–118.

Pearce, J.A., 1996, A user's guide to basalt discrimination diagrams, *in* Wyman, D.A., editor, Trace element geochemistry of volcanic rocks—applications for massive sulphide exploration: Geological Association of Canada Short Course Notes 12, p. 79–113.

Pearce, J.A., Harris, N.G.W., and Tindle, A.G., 1984, Trace element discrimination diagrams for the tectonic interpretation of granitic rocks: Journal of Petrology, v. 25, p. 956–983.

Peterson, F., 1994, Sand dunes, sabkhas, streams, and shallow seas—Jurassic paleogeography in the southern part of the Western Interior basin, *in* Caputo, M.V., Peterson, J.A., and Franczyk, K.J., editors, Mesozoic systems of the Rocky Mountain region, USA: Denver, Colorado, Rocky Mountain Section SEPM (Society for Sedimentary Geology), p. 233–272.

Peterson, F., and Pipiringos, G.N., 1979, Stratigraphic relationships of the Navajo Sandstone to Middle Jurassic formations in parts of southern Utah and northern Arizona: U.S. Geological Survey Professional Paper 1035-B, 43 p.

Phoenix, D.A., 1963, Geology of the Lees Ferry area, Coconino County, Arizona: U.S. Geological Survey Bulletin 1137, 86 p.

Pipiringos, G.N., and O'Sullivan, R.B., 1978, Principal unconformities in Triassic and Jurassic rocks, western interior United States—a preliminary survey: U.S. Geological Survey Professional Paper 1035-A, 29 p.

Riggs, N.R., Mattinson, J.M., and Busby, C.J., 1993, Correlation of Jurassic eolian strata between the magmatic arc and the Colorado Plateau—new U-Pb geochronologic data from southern Arizona: Geological Society of America Bulletin, v. 105, p. 1231–1246.

Schermer, E.R., and Busby, C., 1994, Jurassic magmatism in the central Mojave Desert—implications for arc paleogeography and preservation of continental volcanic sequences: Geological Society of America Bulletin, v. 106, p. 767–790.

Scott, K.M., Macías, J.L., Naranjo, J.A., Rodríguez, S., and McGeehin, J.P., 2001, Catastrophic debris flows transformed from landslides in volcanic terrains—mobility, hazard assessment, and mitigation strategies: U.S. Geological Survey Professional Paper 1630, 59 p.

Siebert, L., Alvarado, G.E., Vallance, J.W., and van Wyk de Vries, B., 2006, Large-volume volcanic edifice failures in Central America and associated hazards, *in* Rose, W.I., Bluth, G.J.S., Carr, M.J., Ewert, J.W., Patino, L.C., and Vallance, J.W., editors, Volcanic hazards in Central America: Geological Society of America Special Paper 412, p. 1–26.

Siebert, L., Glicken, H., and Ui, T., 1987, Volcanic hazards from Bezymianny- and Bandai-type eruptions: Bulletin of Volcanology, v. 49, p. 435–459.

Smith, R.L., 1960, Zones and zonal variations in welded ash flows: U.S. Geological Survey Professional Paper, 354-F, p. 149–159.

Sorensen, S.S., Dunne, G.C., Hanson, R.B., Barton, M.D., Becker, J., Tobisch, O.T., and Fiske, R.S., 1998, From Jurassic shores to Cretaceous plutons—geochemical evidence for paleoalteration environments of metavolcanic rocks, eastern California: Geological Society of America Bulletin, v. 110, p. 326–343.

Sprinkel, D.A., Doelling, H.H., Kowallis, B.J., Waanders, G., and Kuehne, P.A., 2011, Early results of a study of Middle Jurassic strata in the Sevier fold and thrust belt, Utah, *in* Sprinkel, D.A., Yonkee, W.A., and Chidsey, T.C., Jr., editors, Sevier thrust belt—northern and central Utah and adjacent areas: Utah Geological Association Publication 40, p. 151–172.

Sprinkel, D.A., Doelling, H.H., Kowallis, B.J., Waanders, G.L., and Kuehne, P.A., in preparation, Stratigraphy and correlation of the Arapien, Carmel, and Twin Creek Formations (Middle Jurassic) of Utah and surrounding states: Utah Geological Survey Bulletin.

Stewart, J.H., Anderson, T.H., Haxel, G.B., Silver, L.T., and Wright, J.E., 1986, Late Triassic paleogeography of the southern Cordillera—the problem of a source for the voluminous volcanic detritus in the Chinle Formation of the Colorado Plateau region: Geology, v. 14, p. 567–570.

Stewart, J.H., Poole, F.G., and Wilson, R.F., 1972, Stratigraphy and origin of the Chinle Formation and related Upper Triassic strata in the Colorado Plateau region: U.S. Geological Survey Professional Paper 690, 336 p.

Stoenner, R.W., Schaeffer, O.A., and Katcoff, S., 1965, Half-lives of argon-37, argon-39, and argon-42: Science, v. 148, p. 1325–1328.

Taylor, W.J., Bartley, J.M., Fryxell, J.E., Schmitt, J.G., and Vandervoort, D.S., 1993, Tectonic style and regional relations of the central Nevada thrust belt, *in* Lahren, M.M., Trexler, J.H., Jr., and Spinosa C., editors, Crustal evolution of the Great Basin and the Sierra Nevada: Reno, University of Nevada, p. 57–96.

Thompson, A.E., and Stokes, W.L., 1970, Stratigraphy of the San Rafael Group, southwest and south-central Utah: Utah Geological and Mineralogical Survey Bulletin 87, 50 p.

Thorman, C.H., Ketner, K.B., Snoke, A.W., Brooks, W.E., and Mueller, K.J., 1991, Evidence for the involvement of the Roberts Mountains allochthon in Mesozoic tectonics and its effect on mineral deposits and petroleum accumulation models in northeast Nevada, *in* Buffa, R.H., and Coyner,

A.R., editors, Geology and ore deposits of the Great Basin: Geological Society of Nevada, p. 869–905.

Tosdal, R.M., and Wooden, J.L., 2015, Construction of the Jurassic magmatic arc, southeast California and southwest Arizona, *in* Anderson, T.H., Didenko, A.N., Johnson, C.L., Khanchuk, A.I., and MacDonald, J.H., Jr., editors, Late Jurassic margin of Laurasia—a record of faulting accommodating plate rotation: Geological Society of America Special Paper 513, p. 189–221, https://doi.org/10.1130/2015.2513(04).

Voight, B., 1990, The 1985 Nevado del Ruiz volcano catastrophe—anatomy and retrospection: Journal of Volcanology and Geothermal Research, v. 44, p. 349–386.

Wernicke, B., Axen, G.J., and Snow, J.K., 1988, Basin and Range extensional tectonics at the latitude of Las Vegas, Nevada: Geological Society of America Bulletin, v. 100, p. 1738–1757.

Wheatley, D.F., 2018, Clastic pipes and soft-sediment deformation within the Jurassic Carmel Formation, southern Utah—processes, controls, and implication for paleoenvironment, subsurface fluid flow, and a near-surface groundwater system on Mars: Salt Lake City, University of Utah, Ph.D. dissertation, 220 p.

Wheatley, D.F., and Chan, M.A., 2013, Soft-sediment deformation and injectites of the Jurassic Carmel Formation, southern Utah—sedimentary records of strong ground motion [abs.]: Geological Society of America Abstracts with Programs, v. 45, no. 7, p. 126.

Wheatley, D.F., and Chan, M.A., 2018, Clastic pipes and soft-sediment deformation of the Jurassic Carmel Formation, southern Utah, U.S.A.—implications for pipe formation and mechanisms and host-rock controls: Journal of Sedimentary Research, v. 88, p. 1076–1095.

Wheatley, D.F., Chan, M.A., and Sprinkel, D.A., 2016, Clastic pipe characteristics and distributions throughout the Colorado Plateau—implications for paleoenvironment and paleoseismic controls: Sedimentary Geology, v. 344, p. 20–33.

Whitney, J.A., and Stormer, J.C., 1985, Mineralogy, petrology, and magmatic conditions from the Fish Canyon Tuff, central San Juan volcanic field, Colorado: Journal of Petrology, v. 26, p. 726–762.

Wohletz, K., and Heiken, G., 1992, Volcanology and geothermal energy: Berkeley, University of California Press, 432 p.

Wright, J.C., and Dickey, D.D., 1963, Relations of the Navajo and Carmel Formations in southwest Utah and adjoining Arizona: U.S. Geological Survey Professional Paper 450-E, p. E63–E67.

Wright, J.C., Dickey, D.D., and Snyder, R.P., 1979, Measured stratigraphic sections of Jurassic San Rafael Group and adjacent rocks in Kane County, Utah: U.S. Geological Survey Open-File Report 79-1373, 156 p.

Zhang, C., 1996, Volcanic ashes in the Middle Jurassic of southern Utah: Provo, Utah, Brigham Young University, M.S. thesis, 75 p.